ФИЗИКА ЭЛЕМЕНТАРНЫХ ЧАСТИЦ И АТОМНОГО ЯДРА
2009. Т. 40. ВЫП. 5

DIRECT SEARCH FOR DARK MATTER — STRIKING THE BALANCE AND THE FUTURE

V. A. Bednyakov[*]

Joint Institute for Nuclear Research, Dubna

H. V. Klapdor-Kleingrothaus

European Center for Scientific Research, Heidelberg, Germany[**]

[*]E-mail: Vadim.Bednyakov@jinr.ru
[**]Postal address of EuCSR Secretariat: Stahlbergweg 12, 74931 Lobbach, Germany.

ФИЗИКА ЭЛЕМЕНТАРНЫХ ЧАСТИЦ И АТОМНОГО ЯДРА
2009. Т. 40. ВЫП. 5

DIRECT SEARCH FOR DARK MATTER — STRIKING THE BALANCE AND THE FUTURE

V. A. Bednyakov[*]

Joint Institute for Nuclear Research, Dubna

H. V. Klapdor-Kleingrothaus

European Center for Scientific Research, Heidelberg, Germany[**]

Weakly Interacting Massive Particles (WIMPs) are among the main candidates for the relic Dark Matter (DM). The idea of the direct DM detection relies on elastic Spin-Dependent (SD) and Spin-Independent (SI) interactions of WIMPs with target nuclei. In this review paper the relevant formulae for WIMP event rate calculations are collected. For estimations of the WIMP–proton and WIMP–neutron SD and SI cross sections the effective low-energy minimal supersymmetric standard model is used. The traditional one-coupling-dominance approach for evaluation of the exclusion curves is described. Further, the mixed spin-scalar coupling approach is discussed. It is demonstrated, taking the high-spin ^{73}Ge dark matter experiment HDMS as an example, how one can drastically improve the sensitivity of the exclusion curves within the mixed spin-scalar coupling approach, as well as due to a new procedure of background subtraction from the measured spectrum. A general discussion on the information obtained from exclusion curves is given. The necessity of clear WIMP direct detection signatures for a solution of the dark matter problem, is pointed out.

Массивные нейтральные слабовзаимодействующие частицы (WIMPs) являются одним из основных кандидатов на роль реликтовой темной материи (DM). Экспериментальные попытки их прямого детектирования базируются на спин-зависимом (SD) и спин-независимом (SI) характере их упругого взаимодействия с ядрами мишеней расположенных на Земле детекторов. В данном обзоре собраны все необходимые формулы и соотношения для вычисления ожидаемой скорости счета событий прямого детектирования частиц DM. Для вычисления SD- и SI-сечений взаимодействия WIMP-частиц с нуклонами используется низкоэнергетическая версия минимального суперсимметричного расширения стандартной модели. При этом предполагается, что нейтралино, будучи легчайшими суперсимметричными частицами, представляют собой DM-частицы. Описан традиционный подход к получению ограничений на сечения взаимодействия WIMP с нуклонами, основанный на предположении о доминировании только одной константы связи (SD или SI). Далее обсуждается новый подход к анализу DM-данных, одновременно учитывающий ненулевые значения обеих SD- и SI-констант связи WIMP с нуклонами. На примере HDMS эксперимента с высокоспиновым ядром ^{73}Ge показано, как в рамках данного подхода можно значительно улучшить извлекаемые ограничения на интенсивность WIMP-нуклонного взаимодействия. Показано, что такие улучшения можно также получить путем нахождения и вычитания фона из измеряемого спектра. Обсуждается полезность информации, которую обычно получают из ненаблюдения взаимодействия частиц темной материи с ядрами прецизионных детекторов.

[*]E-mail: Vadim.Bednyakov@jinr.ru
[**]Postal address of EuCSR Secretariat: Stahlbergweg 12, 74931 Lobbach, Germany.

Отмечается, что для *действительного* детектирования частиц темной материи необходимо обнаружение отчетливых характерных признаков (сигнатур) взаимодействия WIMP-частиц, а для правильной интерпретации этих сигнатур необходима теоретическая основа, например, суперсимметричная теория.

PACS: 95.30.-k; 95.35.+d; 14.80.Ly; 12.60.Jv

INTRODUCTION

To our knowledge the galactic dark matter particles do not emit any detectable amounts of electromagnetic radiation and manifest themselves only gravitationally by affecting other astrophysical objects. The first evidence of this kind of substance came from the study of galactic rotation curves, i.e., from the measurement of the velocity with which stars, globular stellar clusters, gas clouds, or dwarf galaxies orbit around their centers [1]. If the mass of these galaxies was concentrated in their visible parts, the orbital velocity at large radii r should decrease in accordance with Kepler's law as $1/\sqrt{r}$. Instead, it remains approximately constant to the largest radius where it can be measured. This implies that the total mass $M(r)$ felt by an object at a radius r must increase linearly with r. Studies of this type imply that 90% or more of the mass of the large galaxies is in their dark halos [2–4].

The mass density averaged over the entire Universe is usually expressed in units of the critical density $\rho_c \approx 10^{-29}$ g/cm^3. The dimensionless ratio $\Omega \equiv \rho/\rho_c = 1$ corresponds to a flat Universe. Analyses of galactic rotation curves imply $\Omega \geqslant 0.1$ (see, for example, [5–7]). Studies of clusters and superclusters of galaxies through gravitational lensing or through measurements of their X-ray temperature, as well as studies of the large-scale streaming of galaxies favor larger values of the total mass density of the Universe $\Omega \geqslant 0.3$ (see, for example, [7,8]). Finally, naturalness arguments and most inflationary models prefer $\Omega = 1.0$ to a high accuracy. The requirement that the Universe be at least 10 billion years old implies $\Omega h^2 \leqslant 1$, where h is the present Hubble parameter in units of 100 km/(s $\cdot$ Mpc) [7]. The total density of luminous matter only amounts to less than 0.4% of the critical density [9, 10]. Analyses of Big Bang nucleosynthesis determine the *total* baryonic density to lie in the range $0.017 \leqslant \Omega_b h^2 \leqslant 0.024$ [7]. The upper bound implies $\Omega_b \leqslant 0.05$, in obvious conflict with the lower bound $\Omega \geqslant 0.3$. Most dark matter must therefore be nonbaryonic. Some sort of «new physics» is required to describe this exotic matter, *beyond* the particles described by the Standard Model of particle physics.

Exciting evidence for a flat and accelerating Universe was claimed by [11–13]. The position of the first acoustic peak of the angular power spectrum (of the temperature anisotropy of the cosmic microwave background radiation [14, 15]) strongly suggests a flat Universe with density parameter $\Omega = 1$, while the shape

of the peak is consistent with the density perturbations predicted by models of inflation. Data support $\Omega = \Omega_M + \Omega_\Lambda = 1$, where Ω_M is the matter density in the Universe and Ω_Λ is usually assumed to be a contribution of a nonzero cosmological constant (the energy density of the vacuum). A first claim for the existence of a nonvanishing cosmological constant has been made already in 1986 [16,17]. Recent investigations of the cosmic microwave background temperature anisotropy by the Wilkinson Microwave Anisotropy Probe (WMAP) [18–20] and the galaxy power spectrum with the baryon acoustic peak by the Sloan Digital Sky Survey (SDSS) [21–23] supplied us with the values for the cosmological parameters given in Table 1. The parameters unambiguously confirm the existence of a large amount of dark matter. We omit in this paper discussion of the Dark Energy — another mysterious substance which is connected with the accelerating Universe and fills [9] the gap between a flat Universe and the measured amount of dark matter ($\Omega_{\rm DM} + \Omega_{\rm DE} = \Omega_{\rm tot} = 1$). In 2006, an existing «visualization» of the invisible dark matter substance (see Fig. 1) has been obtained by means of gravitational lensing [24].

Table 1. **Some basic cosmological parameters from WMAP and SDSS [7]**

Hubble constant	$h = 0.704^{+0.015}_{-0.016}$
Baryon density	$\Omega_b h^2 = 0.0219 \pm 0.0007$
Matter density	$\Omega_M h^2 = 0.132 \pm 0.004$
Baryon/Critical density	$\Omega_b = 0.0442 \pm 0.003$
Matter/Critical density	$\Omega_M = 0.249 \pm 0.018$
Total/Critical density	$\Omega_{\rm tot} = 1.011 \pm 0.012$
Age of the Universe, Gyr	$t_0 = 13.7 \pm 0.2$

According to the estimates, based on a detailed model of our Galaxy [25], the local density of DM (nearby the solar system) amounts to about $\rho^{\rm DM}_{\rm local} \simeq 0.3\ {\rm GeV/cm}^3 \simeq 5 \cdot 10^{-25}\ {\rm g/cm}^3$, with an uncertainty within a factor of two [7]. It is assumed to have a Maxwellian velocity distribution in the galactic rest frame with mean velocity $\bar{v} \simeq 270$ km/s [26, 27]. The local flux of DM particles χ is expected to be $\Phi^{\rm DM}_{\rm local} \simeq (100\ {\rm GeV})/m_\chi \cdot 10^5\ {\rm cm}^{-2} \cdot {\rm s}^{-1}$. This value is often considered as a promising basis for direct dark matter search experiments.

Weakly Interacting Massive Particles (WIMPs) are among the most popular candidates for the relic Dark Matter. There is no room for such particles in the Standard Model of particle physics (SM). The lightest supersymmetric (SUSY) particle (LSP), the neutralino (being massive, neutral and stable) is currently often assumed to be a favorite WIMP dark matter particle. The nuclear recoil energy due to elastic WIMP–nucleus scattering is the quantity to be measured by a terrestrial detector in direct DM detection experiments [28]. Detection of the

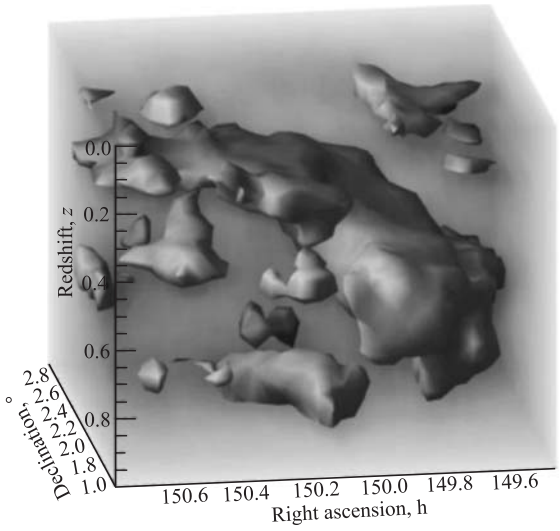

Fig. 1. Three-dimensional reconstruction of the dark matter distribution. It is obtained by the Hubble Space Telescope Collaboration [24] from the differential growth of the gravitational lensing signal between many thin discrete redshift slices. The three axes correspond to right ascension, declination, and redshift. The distance from the Earth increases toward the bottom of the picture. For details see the original paper [24]

very rare events of such WIMP interactions is a challenge for modern particle physics, because of the very weak WIMP coupling with ordinary matter. The rates expected in SUSY models range from 10 to 10^{-7} events per kilogram detector material and day (see, for example, [27, 29–38]). Moreover, for WIMP masses between a few GeV$/c^2$ and 1 TeV$/c^2$, the energy deposited by the recoil nucleus is less than 100 keV. Therefore, in order to be able to detect a WIMP, an experiment with a low-energy threshold and an extremely low radioactive background is required. Furthermore, to indeed detect a WIMP one has to unambiguously register some positive signature of WIMP–nucleus interactions (directional recoil or annual signal modulation) [26, 27]. This means one has to perform a measurement with a detector of large target mass during several years under extremely low radioactive background conditions (see also the discussions of other complications in [39–41]). Despite of all these problems, huge effort is at present put into direct detection of DM particles (see, for example, [2, 7, 42, 43]).

Till now only the DAMA (DArk MAtter) Collaboration claims [44–47] observation of first evidence for a dark matter signal due to registration of the predicted annual modulation of specific shape and amplitude due to the combined motions of the Earth and Sun around the galactic center [26]. Aimed

since more than one decade at the direct detection of DM particles, the DAMA experiment (DAMA/NaI) with 100 kg of highly radio-pure NaI(Tl) scintillator detectors successfully operated till July 2002 at the Gran Sasso National Laboratory (LNGS) of the INFN. On the basis of the results obtained over 7 annual cycles (107731 kg·day total DAMA exposure) the presence of a WIMP-model independent annual modulation signature was observed at a 6.3σ C.L. [46]. The main result of the DAMA observation of the annual modulation signature is a low-mass region of the WIMPs ($40 < m_\chi < 150$ GeV) and relatively high allowed SI or/and SD cross sections (for example, $1 \cdot 10^{-7} < \sigma^p_{\rm SI}(0) < 3 \cdot 10^{-5}$ pb), provided these WIMPs are cold dark matter particles.

Although there are other experiments like EDELWEISS, CDMS, etc., which give sensitive exclusion curves, no one of them at present has the sensitivity to look for the modulation effect. Due to the small target masses and short running times these experiments are unable to see a positive annual modulation signature of the WIMP interactions. Some other experiments with much larger mass targets (mostly NaI) unfortunately are also unable to register the positive signature due to not good enough background conditions (see, for example, [48–50]). Often the results of these and the DAMA experiment have been compared not on the basis of a complete analysis including simultaneously SI and SD WIMP nucleus interaction. This sometimes gives rise to quite some confusion in the literature (for a discussion see [51, 52]), and to attempts to reconcile an artificial DAMA «conflict» with the other experiments [53–59].

Despite of the well-known attempts of the DAMA Collaboration to prove this observation with a new larger NaI setup DAMA/LIBRA [60], it is obvious that such a serious claim should be verified at least by one other completely independent experiment. To confirm this DAMA result one should perform a new experiment which would have (in reasonable time) the same or better sensitivity to the annual modulation signal (and also it would be reasonable to locate this new setup in another low-background underground laboratory). This mission, in particular, could be executed by new-generation experiments with large enough mass of germanium high purity (HP) detectors both with spin (^{73}Ge) and spinless (natural Ge). Despite of obviously necessary strong figthing against backgrounds, the main direction in development of new-generation DM detectors concerns remarkable enlargement of the target mass to be able to observe these positive signatures, and thus to detect DM and to prove, or disprove the DAMA claim. In particular, an enlarged version of the EDELWEISS setup with 40 kg bolometric Ge detectors [61] together with, perhaps, SuperCDMS [62,63], as well as enlarged ZEPLIN [64] or KIMS [65] experiments might become sensitive to the annual modulation in some future.

The main efforts (and expectations) in the present direct dark matter searches are concentrated in the field of the so-called spin-independent (or scalar) interaction of a dark matter WIMP with a target nucleus. This is because it was found

theoretically that for heavy enough nuclei this spin-independent (SI) interaction of DM particles with nuclei usually gives the dominant contribution to the expected event rate of its detection. The reason is the strong (proportional to the squared mass of the target nucleus) enhancement of the SI WIMP–nucleus interaction.

The spin-1/2 WIMP particles, like the LSP neutralinos, interact with ordinary matter predominantly by means of axial vector (spin-dependent) and vector (spin-independent) couplings. There is some revival of interest in the WIMP–nucleus spin-dependent interaction from both theoretical (see, e.g., [35,36,52,66–70]) and experimental (see, e.g., [57, 71–79]) points of view. There are some proposals aimed at direct DM detection with relatively low-mass isotope targets [71, 72, 76–78, 80], as well as some attempts to design and construct a DM detector which is sensitive to the nuclear recoil direction [81–87]. Low-mass targets make preference for the low-mass WIMPs and are more sensitive to the spin-dependent WIMP–nucleus interaction as well [29, 35, 66, 68, 70, 88, 89].

There are at least three reasons to think that SD (or axial-vector) interaction of the DM WIMPs with nuclei could be very important. First, contrary to the only one constraint for SUSY models available from the scalar WIMP–nucleus interaction, the spin WIMP–nucleus interaction supplies us with two such constraints (see, for example, [68] and formulae below). Second, one can notice [35, 36] that even with a very sensitive DM detector (say, with a sensitivity of 10^{-5} events/day/kg) which is sensitive only to the WIMP–nucleus scalar interaction (with spinless target nuclei) one can, in principle, miss a DM signal. To safely avoid such a situation, one should have a spin-sensitive DM detector, i.e., a detector with spin-nonzero target nuclei. Finally, there is a complicated nuclear spin structure, which possesses the so-called long q-tail form-factor behavior. The SI WIMP–nucleus cross section, despite being proportional to A^2, vanishes very quickly (exponentially) with increasing momentum transfer q^2. The SD WIMP–nucleus cross section decreases not so quickly with q^2 and remains still final at the recoil energies ($E_R = q^2/(2M_A)$), where the SI cross section is already zero. Therefore for heavy mass target nuclei and heavy WIMP masses the SD efficiency to detect a DM signal could be much higher than the SI efficiency [66]. Therefore, simultaneous study of both spin-dependent and spin-independent interactions of the DM particles with nuclei significantly increases the chance to observe the DM signal [36, 51, 69, 90].

Following R. Bernabei et al. [45, 46], it was stressed in [51, 52] that for analyzing the data from DM detectors with spin-nonzero targets one should use the so-called mixed spin-scalar coupling approach. This approach is used to demonstrate, taking the high-spin ^{73}Ge detector HDMS [91, 92] as an example, how one can stronger improve the exclusion curves. The mixed spin-scalar coupling approach allowed one to extract information about both SI and SD WIMP–nucleon cross sections analyzing background spectra from the two HDMS setups (prototype and final) simultaneously. This procedure allows an improvement (see our

new analysis in [93]) of the exclusion curves relative to the relevant curves obtained in the traditional one-coupling dominance approach for the HDMS in [79].

The present paper is organized as follows. In the next Section the main formulae for event rate calculations are collected. In Sec. 2 the effective low-energy minimal supersymmetric standard model (effMSSM) is used for calculation of the WIMP–proton and WIMP–neutron SD and SI cross sections. In Sec. 3 the traditional one coupling dominance approach for evaluation of the exclusion curves is discussed. In Sec. 4 the mixed spin-scalar couplings approach is described, the DAMA-inspired exclusion domains for both the above-mentioned couplings are given and compared with SUSY calculations. In Sec. 5 the mixed spin-scalar coupling scheme is applied to the high-spin ^{73}Ge dark matter search experiment HDMS. It is demonstated how one can strongly improve the quality of the exclusion curves within the mixed spin-scalar coupling approach, as well as by using a new procedure of background subtraction from the measured spectrum. In Sec. 6 a general discussion is given. The conclusion summarizes the main items of this review paper.

1. EVENT RATE AND CROSS SECTIONS

Many experiments try to detect directly a relic DM WIMP (or neutralino) χ with mass m_χ via its elastic scattering on a target nucleus (A, Z). The nuclear recoil energy E_R is measured by a proper detector deeply underground (Fig. 2). The differential event rate in respect to the recoil energy (the spectrum) is the subject of the measurements. The rate depends on the density and the velocity distribution of the relic WIMPs in the solar vicinity $f(v)$ and the cross section of WIMP–nucleus elastic scattering [27, 29, 33, 38, 89, 94–96]. The differential event rate per unit mass of the target material has the form

$$\frac{dR}{dE_R} = N_T \frac{\rho_\chi}{m_\chi} \int\limits_{v_{\min}}^{v_{\max}} dv f(v) v \frac{d\sigma^A}{dq^2}(v, q^2). \tag{1}$$

We assume these WIMPs (or neutralinos) to be the dominant component of the DM halo of our Galaxy with a density $\rho_\chi = 0.3$ GeV/cm^3 in the solar vicinity. The (real) nuclear recoil energy $E_R = q^2/(2M_A)$ is typically about $10^{-6} m_\chi$, and N_T is the number density of target nuclei with mass M_A; $v_{\max} = v_{\rm esc} \approx 600$ km/s, $v_{\min} = \left(M_A E_R / 2\mu_A^2\right)^{1/2}$ is the minimal WIMP velocity which still can produce the recoil energy E_R. The WIMP–nucleus differential elastic scattering cross section for spin-nonzero ($J \neq 0$) nuclei contains coherent (spin-independent,

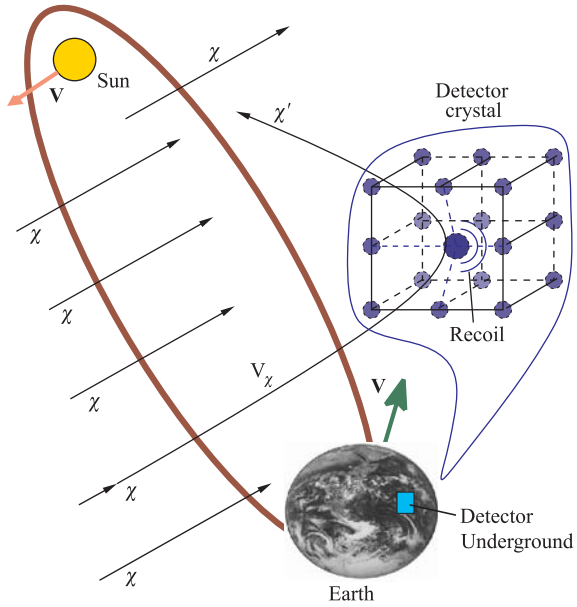

Fig. 2. Detection of the cold dark matter (WIMPs) by elastic scattering from target nuclei in the detector. Due to the expected annual modulation signature of the event rate Eq. (1), the Sun–Earth system is a particularly proper setup for successful direct DM detection

or SI) and axial (spin-dependent, or SD) terms [66, 97, 98]:

$$\frac{d\sigma^A}{dq^2}(v,q^2) = \frac{S^A_{\rm SD}(q^2)}{v^2(2J+1)} + \frac{S^A_{\rm SI}(q^2)}{v^2(2J+1)} = \\ = \frac{\sigma^A_{\rm SD}(0)}{4\mu_A^2 v^2} F^2_{\rm SD}(q^2) + \frac{\sigma^A_{\rm SI}(0)}{4\mu_A^2 v^2} F^2_{\rm SI}(q^2). \quad (2)$$

The normalized ($F^2_{\rm SD,SI}(0) = 1$) finite-momentum-transfer nuclear form-factors $F^2_{\rm SD,SI}(q^2) = \dfrac{S^A_{\rm SD,SI}(q^2)}{S^A_{\rm SD,SI}(0)}$ can be expressed through the nuclear structure functions as follows [66, 97, 98]:

$$S^A_{\rm SI}(q) = \sum_{L\,\text{even}} |\langle J||\mathcal{C}_L(q)||J\rangle|^2 \simeq |\langle J||\mathcal{C}_0(q)||J\rangle|^2, \\ S^A_{\rm SD}(q) = \sum_{L\,\text{odd}} \left(|\langle N||\mathcal{T}^{el5}_L(q)||N\rangle|^2 + |\langle N||\mathcal{L}^5_L(q)||N\rangle|^2\right). \quad (3)$$

The explicit form of the transverse electric $\mathcal{T}^{\rm el5}(q)$ and longitudinal $\mathcal{L}^5(q)$ multipole projections of the axial vector current operator and the scalar function $\mathcal{C}_L(q)$ can be found in [66,70,97–99]. For $q=0$ the nuclear SD and SI cross sections can be presented as follows:

$$\sigma^A_{\rm SI}(0)=\frac{4\mu_A^2 S_{\rm SI}(0)}{(2J+1)}=\frac{\mu_A^2}{\mu_p^2}A^2\sigma^p_{\rm SI}(0), \tag{4}$$

$$\sigma^A_{\rm SD}(0)=\frac{4\mu_A^2 S_{\rm SD}(0)}{(2J+1)}=\frac{4\mu_A^2}{\pi}\frac{(J+1)}{J}\left\{a_p\langle \mathbf{S}^A_p\rangle+a_n\langle \mathbf{S}^A_n\rangle\right\}^2, \tag{5}$$

$$=\frac{\mu_A^2}{\mu_p^2}\frac{4}{3}\frac{J+1}{J}\sigma^{pn}_{\rm SD}(0)\left\{\langle \mathbf{S}^A_p\rangle\cos\theta+\langle \mathbf{S}^A_n\rangle\sin\theta\right\}^2. \tag{6}$$

Following Bernabei et al. [45,46] the effective spin WIMP–nucleon cross section $\sigma^{pn}_{\rm SD}(0)$ and the coupling mixing angle θ were introduced

$$\sigma^{pn}_{\rm SD}(0)=\frac{\mu_p^2}{\pi}\frac{4}{3}\Big[a_p^2+a_n^2\Big],\qquad \tan\theta=\frac{a_n}{a_p}; \tag{7}$$

$$\sigma^p_{\rm SD}=\sigma^{pn}_{\rm SD}\cdot\cos^2\theta,\quad \sigma^n_{\rm SD}=\sigma^{pn}_{\rm SD}\cdot\sin^2\theta. \tag{8}$$

Here, $\mu_A=\dfrac{m_\chi M_A}{m_\chi+M_A}$ is the reduced mass of the neutralino and the nucleus, and it is assumed that $\mu_n^2=\mu_p^2$. The dependence on effective WIMP–quark (in SUSY neutralino–quark) couplings $\mathcal{C}_q$ and $\mathcal{A}_q$ in the underlying theory

$$\mathcal{L}_{\rm eff}=\sum_q\left(\mathcal{A}_q\bar\chi\gamma_\mu\gamma_5\chi\bar q\gamma^\mu\gamma_5 q+\mathcal{C}_q\bar\chi\chi\bar qq\right)+\ldots \tag{9}$$

and on the spin $\left(\Delta_q^{(p,n)}\right)$ and the mass or scalar $\left(f_q^{(p)}\approx f_q^{(n)}\right)$ structure of the proton and neutron enters into these formulae via the zero-momentum-transfer WIMP–proton and WIMP–neutron SI and SD cross sections:

$$\sigma^p_{\rm SI}(0)=4\frac{\mu_p^2}{\pi}c_0^2,\qquad c_0=c_0^{p,n}=\sum_q\mathcal{C}_q f_q^{(p,n)}; \tag{10}$$

$$\sigma^{p,n}_{\rm SD}(0)=12\frac{\mu_{p,n}^2}{\pi}a_{p,n}^2,\qquad a_p=\sum_q\mathcal{A}_q\Delta_q^{(p)},\quad a_n=\sum_q\mathcal{A}_q\Delta_q^{(n)}. \tag{11}$$

The factors $\Delta_q^{(p,n)}$, which parameterize the quark spin content of the nucleon, are defined as $2\Delta_q^{(n,p)}s^\mu\equiv\langle p,s|\bar\psi_q\gamma^\mu\gamma_5\psi_q|p,s\rangle_{(p,n)}$. The quantity $\langle \mathbf{S}^A_{p(n)}\rangle$ denotes the total spin of protons (neutrons) averaged over all A nucleons of the

nucleus (A, Z):

$$\langle \mathbf{S}^A_{p(n)} \rangle \equiv \langle A|\mathbf{S}^A_{p(n)}|A\rangle = \left\langle A \left| \sum_i^A \mathbf{s}^i_{p(n)} \right| A \right\rangle . \tag{12}$$

The mean velocity $\langle v \rangle$ of the relic neutralinos of our Galaxy is about $300\ \mathrm{km/s} = 10^{-3}$ c. Assuming $q_{\max} R \ll 1$, where R is the nuclear radius and $q_{\max} = 2\mu_A v$ is the maximum of the momentum transfer in the process of the χA scattering,

Table 2. **Zero momentum spin structure of nuclei in different models. The measured magnetic moments used as input are enclosed in parentheses. The variation of the $\langle \mathbf{S}^A_p \rangle$ and $\langle \mathbf{S}^A_n \rangle$ for fixed A reflects the level of inaccuracy and complexity of the current nuclear structure calculations [70]**

Different models	$\langle \mathbf{S}_p \rangle$	$\langle \mathbf{S}_n \rangle$	μ (in μ_N)
^{73}Ge ($L_J = G_{9/2}$)			
ISPSM, Ellis–Flores [103, 104]	0	0.5	-1.913
OGM, Engel–Vogel [105]	0	0.23	$(-0.879)_{\mathrm{exp}}$
IBFM, Iachello et al. [106] and [98]	-0.009	0.469	-1.785
IBFM (quenched), Iachello et al. [106] and [98]	-0.005	0.245	$(-0.879)_{\mathrm{exp}}$
TFFS, Nikolaev–Klapdor-Kleingrothaus [107]	0	0.34	—
SM (small), Ressell et al. [98]	0.005	0.496	-1.468
SM (large), Ressell et al. [98]	0.011	0.468	-1.239
SM (large, quenched), Ressell et al. [98]	0.009	0.372	$(-0.879)_{\mathrm{exp}}$
«Hybrid» SM, Dimitrov et al. [108]	0.030	0.378	-0.920
^{127}I ($L_J = D_{5/2}$)			
ISPSM, Ellis–Flores [104, 109]	1/2	0	4.793
OGM, Engel–Vogel [105]	0.07	0	$(2.813)_{\mathrm{exp}}$
IBFM, Iachello et al. [106]	0.464	0.010	$(2.813)_{\mathrm{exp}}$
IBFM (quenched), Iachello et al. [106]	0.154	0.003	$(2.813)_{\mathrm{exp}}$
TFFS, Nikolaev–Klapdor-Kleingrothaus [107]	0.15	0	—
SM (Bonn A), Ressell–Dean [101]	0.309	0.075	2.775 $\{2.470\}_{\mathrm{eff}}$
SM (Nijmegen II), Ressell–Dean [101]	0.354	0.064	3.150 $\{2.7930\}_{\mathrm{eff}}$
^{131}Xe ($L_J = D_{3/2}$)			
ISPSM, Ellis–Flores [103, 104]	0	-0.3	1.148
OGM, Engel–Vogel [105]	0.0	-0.18	$(0.692)_{\mathrm{exp}}$
IBFM, Iachello et al. [106]	0.000	-0.280	$(0.692)_{\mathrm{exp}}$
IBFM (quenched), Iachello et al. [106]	0.000	-0.168	$(0.692)_{\mathrm{exp}}$
TFFS, Nikolaev–Klapdor-Kleingrothaus [107]		-0.186	—
SM (Bonn A), Ressell–Dean [101]	-0.009	-0.227	0.980 $\{0.637\}_{\mathrm{eff}}$
SM (Nijmegen II), Ressell–Dean [101]	-0.012	-0.217	0.979 $\{0.347\}_{\mathrm{eff}}$
QTDA, Engel [66]	-0.041	-0.236	0.70

the spin-dependent matrix element takes a simple form (*zero momentum transfer limit*) [100, 101]:

$$\mathcal{M} = C\langle A|a_p\mathbf{S}_p + a_n\mathbf{S}_n|A\rangle \cdot \mathbf{s}_\chi = C\Lambda\langle A|\mathbf{J}|A\rangle \cdot \mathbf{s}_\chi. \tag{13}$$

Here, $\mathbf{s}_\chi$ denotes the spin of the neutralino, and

$$\Lambda = \frac{\langle N|a_p\mathbf{S}_p + a_n\mathbf{S}_n|N\rangle}{\langle N|\mathbf{J}|N\rangle} = \frac{\langle N|(a_p\mathbf{S}_p + a_n\mathbf{S}_n)\cdot\mathbf{J}|N\rangle}{J(J+1)} = \\ = \frac{a_p\langle\mathbf{S}_p\rangle}{J} + \frac{a_n\langle\mathbf{S}_n\rangle}{J}. \tag{14}$$

Note a coupling of the spin of χ to the spin carried by the protons and the neutrons. The uncertainties arising from the electroweak and QCD scale physics are incorporated in the factors a_p and a_n. The normalization factor C involves the coupling constants, the masses of the exchanged bosons, and the mixing parameters relevant to the lightest supersymmetric particle (LSP), i.e., it is not related to the associated nuclear matrix elements [102]. In the limit of zero momentum transfer $q = 0$, the spin structure function in Eq. (3) reduces to the form

$$S^A(0) = \frac{1}{4\pi}\left|\left\langle A\left|\left|\sum_i \frac{1}{2}(a_0 + a_1\tau_3^i)\boldsymbol{\sigma}_i\right|\right|A\right\rangle\right|^2 = \frac{2J+1}{\pi}J(J+1)\Lambda^2.$$

For the most interesting isotopes either $\langle\mathbf{S}_p^A\rangle$ or $\langle\mathbf{S}_n^A\rangle$ dominates ($\langle\mathbf{S}_{n(p)}^A\rangle \ll \langle\mathbf{S}_{p(n)}^A\rangle$). See, for example, Table 2.

The differential event rate (1) can be given also in the form [46, 51]:

$$\frac{dR(E_R)}{dE_R} = \kappa_{\rm SI}(E_R, m_\chi)\,\sigma_{\rm SI} + \kappa_{\rm SD}(E_R, m_\chi)\,\sigma_{\rm SD}, \tag{15}$$

$$\kappa_{\rm SI}(E_R, m_\chi) = N_T\frac{\rho_\chi M_A}{2m_\chi\mu_p^2}B_{\rm SI}(E_R)\left[M_A^2\right], \\ \kappa_{\rm SD}(E_R, m_\chi) = N_T\frac{\rho_\chi M_A}{2m_\chi\mu_p^2}B_{\rm SD}(E_R)\left[\frac{4}{3}\frac{J+1}{J}\left(\langle\mathbf{S}_p\rangle\cos\theta + \langle\mathbf{S}_n\rangle\sin\theta\right)^2\right], \tag{16}$$

$$B_{\rm SI,SD}(E_R) = \frac{\langle v\rangle}{\langle v^2\rangle}F_{\rm SI,SD}^2(E_R)I(E_R).$$

The dimensionless integral $I(E_R)$ is a dark-matter-particle velocity distribution correction (see Eq. (15)):

$$I(E_R) = \frac{\langle v^2 \rangle}{\langle v \rangle} \int\limits_{x_{\min}} \frac{f(x)}{v} dx =$$

$$= \frac{\sqrt{\pi}}{2} \frac{3 + 2\eta^2}{\sqrt{\pi}(1 + 2\eta^2)\,\mathrm{erf}\,(\eta) + 2\eta\,\mathrm{e}^{-\eta^2}} [\mathrm{erf}\,(x_{\min} + \eta) - \mathrm{erf}\,(x_{\min} - \eta)], \quad (17)$$

where one assumes that in the rest frame of our Galaxy WIMPs have a Maxwell–Boltzmann velocity distribution, and uses the dimensionless Earth speed with respect to the halo η, as well as $x^2_{\min} = \frac{3}{4} \frac{M_A E_R}{\mu_A^2 \bar{v}^2}$ [26, 27]. The error function is $\mathrm{erf}(x) = \frac{2}{\sqrt{\pi}} \int\limits_0^x dt\,\mathrm{e}^{-t^2}$. The velocity variable is the dispersion $\bar{v} \simeq 270$ km/c. The mean WIMP velocity $\langle v \rangle = \sqrt{5/3}\bar{v}$. We also assume both form-factors $F^2_{\mathrm{SI,SD}}(E_R)$ in the simplest Gaussian form following [103, 104]. In particular, this allows rather simple formulae (see Eq. (16)) to be used. Integrating the differential rate Eq. (1) from the recoil energy threshold ϵ to some maximal energy ε one obtains the total detection rate $R(\epsilon, \varepsilon)$ as a sum of the SD and SI terms:

$$R(\epsilon, \varepsilon) = R_{\mathrm{SI}}(\epsilon, \varepsilon) + R_{\mathrm{SD}}(\epsilon, \varepsilon) =$$

$$= \int\limits_{\epsilon}^{\varepsilon} dE_R \kappa_{\mathrm{SI}}(E_R, m_\chi)\,\sigma_{\mathrm{SI}} + \int\limits_{\epsilon}^{\varepsilon} dE_R \kappa_{\mathrm{SD}}(E_R, m_\chi)\,\sigma_{\mathrm{SD}}. \quad (18)$$

To accurately estimate the event rate $R(\epsilon, \varepsilon)$ one needs to know a number of quite uncertain astrophysical and nuclear structure parameters as well as the very specific characteristics of an experimental setup (see, for example, discussions in [46, 110]).

As m_χ increases, the product qR starts to become non-negligible and *the finite momentum transfer limit* must be considered [70, 97–99, 101]. The formalism is a straightforward extension of that developed for the study of weak and electromagnetic semileptonic interactions in nuclei [98, 101]. With the isoscalar spin coupling constant $a_0 = a_n + a_p$ and the isovector spin coupling constant $a_1 = a_p - a_n$ one can split the nuclear structure function $S^A(q)$ (from Eqs. (2) and (3)) into a pure isoscalar term, $S^A_{00}(q)$, a pure isovector term, $S^A_{11}(q)$, and an interference term, $S^A_{01}(q)$, in the following way:

$$S^A(q) = a_0^2 S^A_{00}(q) + a_1^2 S^A_{11}(q) + a_0 a_1 S^A_{01}(q). \quad (19)$$

The relations $S^A_{00}(0) = C(J)(\langle \mathbf{S}_p \rangle + \langle \mathbf{S}_n \rangle)^2$, $S^A_{11}(0) = C(J)(\langle \mathbf{S}_p \rangle - \langle \mathbf{S}_n \rangle)^2$, and $S^A_{01}(0) = 2C(J)(\langle \mathbf{S}^2_p \rangle - \langle \mathbf{S}^2_n \rangle)$ with $C(J) = \dfrac{2J+1}{4\pi}\dfrac{J+1}{J}$, connect the nuclear spin structure function $S^A(q=0)$ with proton $\langle \mathbf{S}_p \rangle$ and neutron $\langle \mathbf{S}_n \rangle$ spin contributions averaged over the nucleus [99].

These three partial structure functions $S^A_{ij}(q)$ allow calculation of spin-dependent cross sections for any heavy Majorana particle as well as for the neutralino with arbitrary composition [100].

The first model to estimate the spin content in the nucleus for the dark matter search was the independent single-particle shell model (ISPSM) used originally by Goodman and Witten [28] and later in [94,103,111]. There are several approaches to more accurate calculations of the nuclear structure effects relevant to the dark matter detection. The list of the models includes the Odd Group Model (OGM) of Engel and Vogel [105] and their extended OGM (EOGM) [97, 105]; Interacting Boson Fermion Model (IBFM) of Iachello, Krauss, and Maino [106]; Theory of Finite Fermi Systems (TFFS) of Nikolaev and Klapdor-Kleingrothaus [107]; Quasi-Tamm–Dancoff Approximation (QTDA) of Engel [66]; different shell model treatments (SM) by Pacheco and Strottman [112]; by Engel, Pittel, Ormand, and Vogel [113] and Engel, Ressell, Towner, and Ormand, [100], by Ressell et al. [98] and Ressell and Dean [101]; by Kosmas, Vergados et al. [31, 88, 114]; the so-called «hybrid» model of Dimitrov, Engel, and Pittel [108] and perturbation theory based on calculations of Engel et al. [100]. For the experimentally interesting nuclear systems ^{29}Si and ^{73}Ge very elaborate calculations have been performed by Ressell et al. [98]. In the case of ^{73}Ge a further improved calculation by Dimitrov, Engel, and Pittel was carried out [108] by suitably mixing variationally determined triaxial Slater determinants. At the present time the necessity for more detailed calculations *especially* for the spin-dependent component of the cross sections for heavy nuclei is well motivated.

To perform modern data analysis in the finite momentum transfer approximation it looks reasonable to use formulae for the differential event rate (Eq. (1)) as schematically given below:

$$\frac{dR(\epsilon,\varepsilon)}{dE_R} = \mathcal{N}(\epsilon,\varepsilon,E_R,m_\chi)\left[\eta_{\rm SI}(E_R,m_\chi)\,\sigma^p_{\rm SI} + \eta'_{\rm SD}(E_R,m_\chi,\omega)\,a_0^2\right]; \quad (20)$$

$$\mathcal{N}(\epsilon,\varepsilon,E_R,m_\chi) = \left[N_T\frac{c\rho_\chi}{2m_\chi}\frac{M_A}{\mu_p^2}\right]\frac{4\mu_A^2}{\langle q^2_{\rm max}\rangle}\left\langle\frac{v}{c}\right\rangle I(E_R)\theta(E_R-\epsilon)\theta(\varepsilon-E_R),$$

$$\eta_{\rm SI}(E_R,m_\chi) = \left\{A^2F^2_{\rm SI}(E_R)\right\};$$

$$\eta'_{\rm SD}(E_R,m_\chi,\omega) = \mu_p^2\left\{\frac{4}{2J+1}\left(S_{00}(q)+\omega^2\,S_{11}(q)+\omega\,S_{01}(q)\right)\right\}.$$

Here the ratio of isovector-to-isoscalar nucleon couplings is $\omega = a_1/a_0$. The detector threshold recoil energy ϵ and the maximal available recoil energy ε ($\epsilon \leqslant E_R \leqslant \varepsilon$) have been introduced already in Eq. (18). In practice, for example, with an ionization or scintillation signal, one has to take into account the quenching of the recoil energy, when the visible recoil energy is smaller than the real recoil energy transmitted by the WIMP to the target nucleus.

Formulae (20) allow experimental recoil spectra to be directly described in terms of only *three* [68] (it is rather reasonable to assume $\sigma^p_{\rm SI}(0) \approx \sigma^n_{\rm SI}(0)$) independent parameters ($\sigma^p_{\rm SI}$, a_0^2, and ω) for any fixed WIMP mass m_χ and any neutralino composition. Comparing this formula with the observed recoil spectra for different targets (Ge, Xe, F, NaI, etc.) one can directly and simultaneously restrict both isoscalar c_0 (via $\sigma^p_{\rm SI}$) and isovector neutralino–nucleon effective couplings $a_{0,1}$. These constraints, based on the nuclear spin structure functions for finite q, will impose *the most model-independent and most accurate restrictions* on any SUSY parameter space. Contrary to some other possibilities (see, for example, [46] and [115]), this procedure is direct and uses as much as possible the results of the accurate nuclear spin structure calculations.

It is seen from Eqs. (8) and (20) that the SD cross sections $\sigma^p_{\rm SD}$ and $\sigma^n_{\rm SD}$ (or equivalently a_0^2 and $\omega = a_1/a_0$) are the only two WIMP–nucleon spin variables which can be constrained (or extracted) from DM measurements. Therefore there is no sense to extract from the data (with «artificial» twofold ambiguity) effective WIMP–nucleon couplings a_p and a_n.

2. CROSS SECTIONS IN THE EFFECTIVE LOW-ENERGY MSSM

To estimate the expected direct DM detection rates (with formulae (1), (18) or (20)) one should calculate cross sections $\sigma_{\rm SI}$ and $\sigma_{\rm SD}$ (or WIMP–nucleon couplings c_0 and $a_{p,n}$) within the framework of some SUSY-based theory or take them from some experimental data (if it is possible).

To obtain as much as general SUSY predictions it appeared more convenient to work within a phenomenological effective low-energy minimal SUSY model (effMSSM) whose parameters are defined directly at the electroweak scale, relaxing completely constraints following from any unification assumption (see, for example, [8, 30, 33, 35, 36, 38, 69, 89, 116–124]). The effMSSM parameter space is determined by entries of the mass matrices of neutralinos, charginos, Higgs bosons, sleptons, and squarks. The list of free parameters includes $\tan\beta$, the ratio of neutral Higgs boson vacuum expectation values; μ, the bilinear Higgs parameter of the superpotential; $M_{1,2}$, soft gaugino masses; M_A, the CP-odd Higgs mass; $m^2_{\widetilde{Q}}$, $m^2_{\widetilde{U}}$, $m^2_{\widetilde{D}}$ ($m^2_{\widetilde{L}}$, $m^2_{\widetilde{E}}$), squark (slepton) mass parameters squared for the 1st and 2nd generation; $m^2_{\widetilde{Q}_3}$, $m^2_{\widetilde{T}}$, $m^2_{\widetilde{B}}$ ($m^2_{\widetilde{L}_3}$, $m^2_{\widetilde{\tau}}$), squark (slepton) mass parameters squared for the 3rd generation; A_t, A_b, A_τ, soft trilinear couplings

for the 3rd generation. The third gaugino mass parameter M_3 defines the mass of the gluino in the model and is determined by means of the GUT assumption $M_2 = 0.3M_3$. In the MSSM the lightest neutralino $\chi \equiv \tilde{\chi}_1^0$ is a mixture of four superpartners of gauge and Higgs bosons (Bino, Wino, and two Higgsinos): $\chi = N_{11}\widetilde{B}^0 + N_{12}\widetilde{W}^0 + N_{13}\widetilde{H}_1^0 + N_{14}\widetilde{H}_2^0$. Concerning the neutralino composition it is commonly accepted that χ is mostly gaugino-like if $P \equiv N_{11}^2 + N_{12}^2 > 0.9$ and Higgsino-like if $P < 0.1$, or mixed otherwise.

To constrain the huge effMSSM parameter space and to have reliable predictions for the dark matter experiments one usually takes into account available information from colliders, astrophysics and rare decays. In our previous considerations [35,36,69,121–124] the experimental upper limits on sparticle and Higgs masses from their nonobservations [7,125] were included. Also the limits on the rare $b \to s\gamma$ decay [126,127] following [128–131] have been imposed.

Furthermore, for each point in the MSSM parameter space (MSSM model), the relic density of the light neutralinos $\Omega_\chi h^2$ was evaluated with the code [121–123] based on the code DarkSUSY [132] with the allowance for all coannihilation channels with two-body final states that can occur between neutralinos, charginos, sleptons, stops, and sbottoms as long as their masses are $m_i < 2m_\chi$. Two cosmologically interesting regions were considered. One is $0.1 < \Omega_\chi h^2 < 0.3$ and the other is the WMAP-inspired region $0.094 < \Omega_\chi h^2 < 0.129$ [18,19]. The possibility the LSP to be not the only DM candidate, with much smaller relic density $0.002 < \Omega h^2 < 0.1$, is also taken into account. Further details can be found in [51]. In numerical studies of [35,121–123,133] the parameters of the effMSSM are randomly varied in the following intervals:

$$\begin{gathered} -1 < M_1 < 1 \text{ TeV}, \quad -2 < M_2, \mu, A_t < 2 \text{ TeV}, \\ 1 < \tan\beta < 50, \quad 60 < M_A < 1000 \text{ GeV}, \\ 10 < m_Q^2, m_L^2, m_{Q_3}^2, m_{L_3}^2 < 10^6 \text{ GeV}^2. \end{gathered} \tag{21}$$

For the other sfermion mass parameters as before in [35,36,69,121–124] we used the relations $m_{\widetilde{U}}^2 = m_{\widetilde{D}}^2 = m_{\widetilde{Q}}^2$, $m_{\widetilde{E}}^2 = m_{\widetilde{L}}^2$, $m_{\widetilde{T}}^2 = m_{\widetilde{B}}^2 = m_{\widetilde{Q}_3}^2$, $m_{\widetilde{E}_3}^2 = m_{\widetilde{L}_3}^2$. The parameters A_b and A_τ are fixed to be zero. We consider the domain of the MSSM parameter space, in which we perform our scans, as quite spread and natural.

Typical WIMP–nucleon cross sections of both spin (SD) and scalar (SI) interactions as function of the WIMP mass are shown as scatter plots in Fig. 3. In the figure open circles correspond to cross sections calculated under the old assumption that $0.025 < \Omega_\chi h^2 < 1$. Filled triangles give the same cross section but the constraint on the flat and accelerating Universe is imposed by $0.1 < \Omega_\chi h^2 < 0.3$. One can see that the reduction of the allowed domain for the relic density does not significantly affect spin-dependent and the spin-independent WIMP–nucleon cross sections. The different behavior of SD and SI cross sections

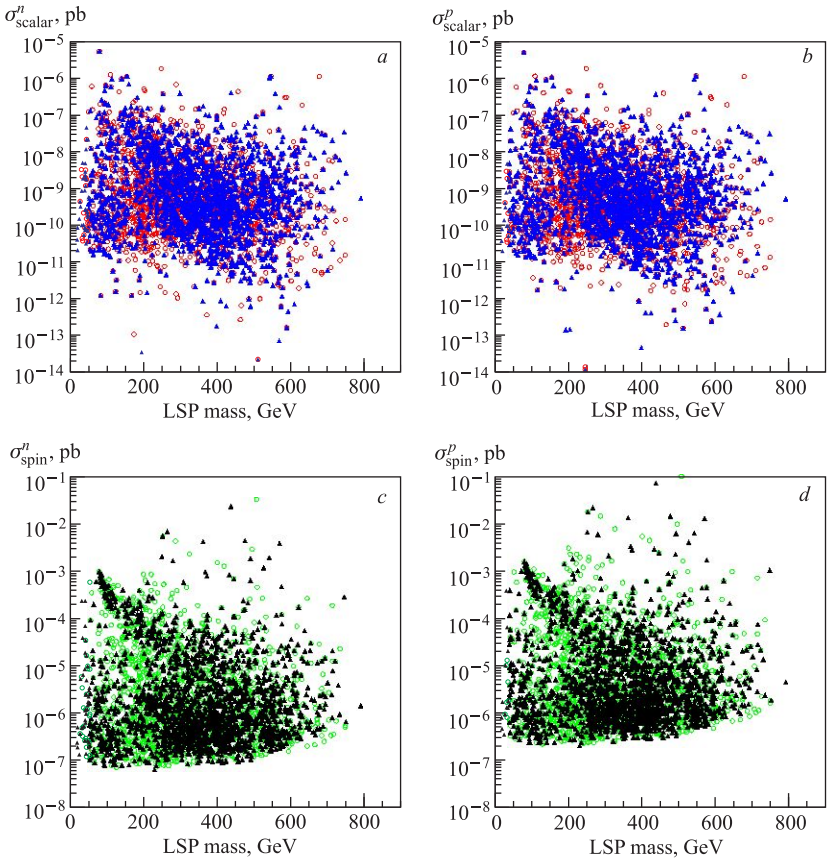

Fig. 3. Cross sections of spin-dependent and spin-independent interactions of WIMPs with proton and neutron. Filled triangles (open circles) correspond to relic neutralino density $0.1 < \Omega_\chi h^2 < 0.3$ ($0.025 < \Omega_\chi h^2 < 1$). From [35, 121–123, 133]

with mass of the LSP can be seen from the plots. There is a more stringent lower bound for the spin-dependent cross section. It is at a level of 10^{-7} pb.

For more accurate investigation of the DAMA-inspired domain of the lower masses of the LSP ($m_\chi < 200$ GeV) in [51] both σ_{SD} and σ_{SI} have also been calculated within the effMSSM. To this end the intervals of the randomly scanned MSSM parameter space in [51] were narrowed:

$$-200 < M_1 < 200 \text{ GeV}, \quad -1 < M_2, \mu < 1 \text{ TeV}, \quad 50 < M_A < 500 \text{ GeV}. \quad (22)$$

The results of these evaluations are shown as scatter plots in Fig. 4, which is the WIMP low-mass update of Fig. 3. In Fig. 4 filled circles correspond to cross

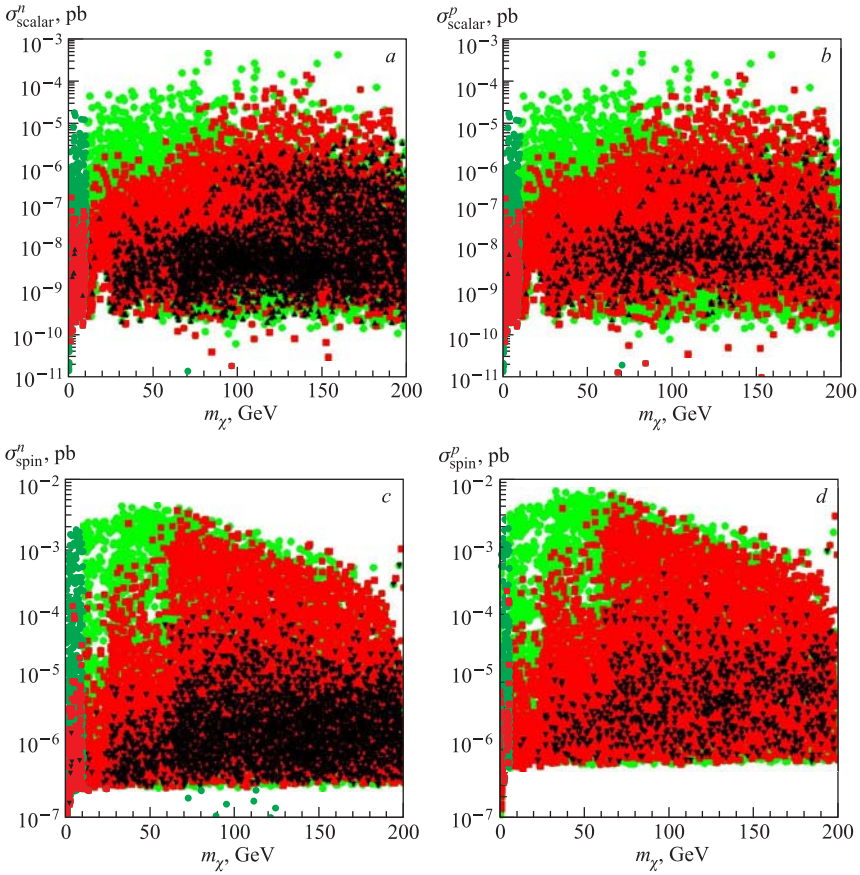

Fig. 4. Cross sections of the spin-dependent (spin) and the spin-independent (scalar) interactions of WIMPs with the proton and the neutron. Filled circles correspond to the relic neutralino density $0 < \Omega_\chi h_0^2 < 1$, squares correspond to the subdominant relic neutralino contribution $0.002 < \Omega_\chi h_0^2 < 0.1$ and triangles correspond to the relic neutralino density $0.1 < \Omega_\chi h_0^2 < 0.3$ (*a*) and to the WMAP relic density $0.094 < \Omega_\chi h_0^2 < 0.129$ (*b*)

sections calculated when the neutralino relic density should just not overclose the Universe ($0.0 < \Omega_\chi h_0^2 < 1.0$). Filled squares show the same cross sections when one assumes the relic neutralinos to be not the only DM particles and give only a subdominant contribution to the relic density $0.002 < \Omega_\chi h_0^2 < 0.1$. In Fig. 4, *a* these cross sections are shown with the black triangles corresponding to the case when the relic neutralino density is in the bounds previously associated with the so-called flat and accelerating Universe $0.1 < \Omega_\chi h_0^2 < 0.3$. The black triangles in

Fig. 4, *b* correspond to the the WMAP and SDSS [18,19] constraint on the matter relic density $0.094 < \Omega_\chi h_0^2 < 0.129$ imposed in 2004. Despite a visible reduction of the allowed domain for the relic density due to the WMAP+SDSS result the upper bounds for the spin-dependent and the spin-independent WIMP–nucleon cross section are not significantly affected.

Finally, it is perhaps the right place here to comment the following. Unfortunately the MSSM parameter space is huge and to obtain some reliable feeling, concerning, for example, the expected rate of dark-matter detection when all relevant experimental and cosmological constraints are taken into account, one has nothing but this statistical numerical method (see, for example, [29,38,89,95,96,119,134,135]). This method allows lower and upper bounds for any observable to be estimated, and to make conclusions about the prospects for dark-matter detection with present or future high-accuracy dark-matter detectors. The larger the amount of points which confirm such a conclusion the better. The conclusions we made here are based on hundreds of thousands of points which passed all constraints. Of course, we have no proved protection against peculiar choices of parameters which could lead to some cancellation and to small cross sections even if Higgs masses are small. Nevertheless, the probability of these choices is very small (about 1/100000), otherwise we should already meet them with our random scanning. On the other side, if these peculiar choices exist and one day would manifest themselves, this would be a very interesting puzzle, because it would be some kind of fine tuning of parameters, which requires strong further development of our understanding of the theory [124].

3. ONE-COUPLING DOMINANCE APPROACH

From the definitions of SD and SI WIMP–nucleus and WIMP–nucleon cross sections (Eqs. (4)–(8), (10) and (11)) one can conclude that the spin observables in DM search give us two independent constraints on a SUSY model via $\sigma^p_{\rm SD}(0)$ and $\sigma^n_{\rm SD}(0)$, or, equivalently, via a_p and a_n (or a_0 and a_1). These constraints are usually presented in the form of exclusion curves obtained with different target nuclei and recalculated in terms of nuclear-independent $\sigma^p_{\rm SD}(0)$ (see, for example, Fig. 5) and $\sigma^n_{\rm SD}(0)$ (see, for example, Fig. 6). For a fixed mass of the WIMP the cross sections of SI or SD elastic WIMP–nucleon interaction located above these curves are excluded.

This simple presentation allows one to compare directly sensitivities of DM experiments with different nuclear targets. At the current level of accuracy (when $f_q^{(p)} \approx f_q^{(n)}$ and $\sigma^p_{\rm SI}(0) \approx \sigma^n_{\rm SI}(0)$, see Fig. 3) there is *only one* constraint for a WIMP–nucleon cross section (Fig. 7) from spin-independent DM search experiments. Indeed, for the spin-zero nuclear target the experimentally measured event rate (Eq. (1)) of direct DM particle detection, via formula (2), is connected

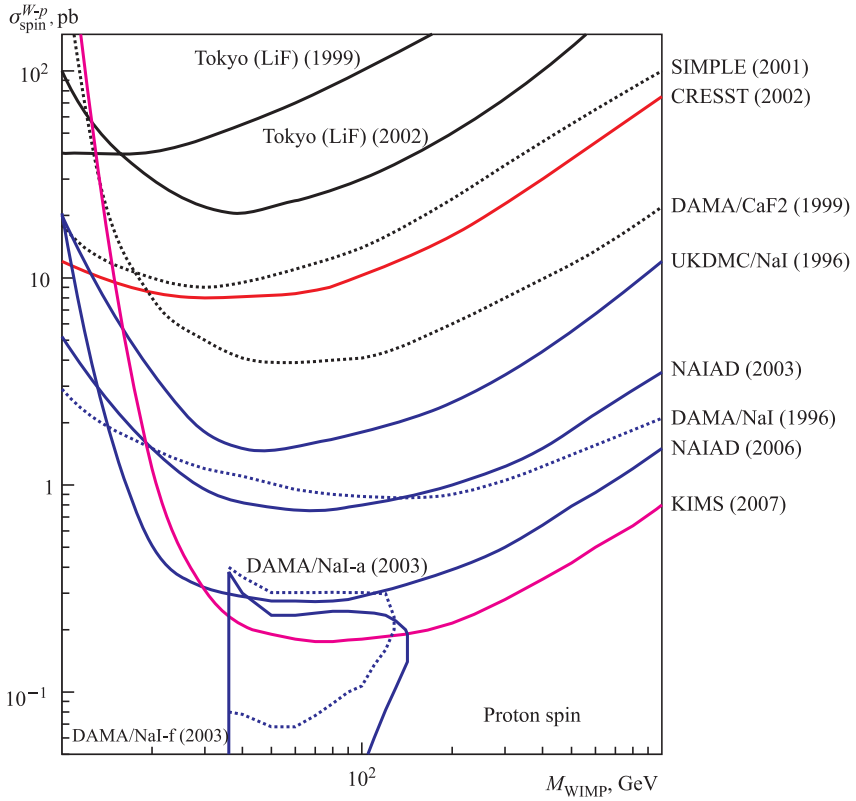

Fig. 5. Exclusion curves for the spin-dependent WIMP–proton cross sections σ^p_{SD} as a function of the WIMP mass. All curves, except the NAIAD and Tokyo-LiF, are obtained in the one-coupling dominance approach with $\sigma_{\text{SI}} = 0$ and $\sigma^n_{\text{SD}} = 0$. The DAMA/NaI-a(f) contours for the WIMP–proton SD interaction in ^{127}I are obtained on the basis of the positive signature of annual modulation within the framework of the mixed scalar-spin coupling approach [45, 46]. For details see [51]

with the zero-momentum WIMP–proton(neutron) cross section (4). The zero momentum scalar WIMP–proton(neutron) cross section $\sigma^p_{\text{SI}}(0)$ can be expressed through effective neutralino–quark couplings $\mathcal{C}_q$ (9) by means of expression (10). These couplings $\mathcal{C}_q$ (as well as $\mathcal{A}_q$) can be directly connected with the fundamental parameters of a SUSY model such as $\tan\beta$, $M_{1,2}$, μ, masses of sfermions and Higgs bosons, etc. Therefore experimental limitations on the SI neutralino–nucleon cross section supply us with a constraint on the fundamental parameters of an underlying SUSY model. In the case of the SD WIMP–nucleus interaction from a measured differential rate Eq. (1) one first extracts a limitation for $\sigma^A_{\text{SD}}(0)$,

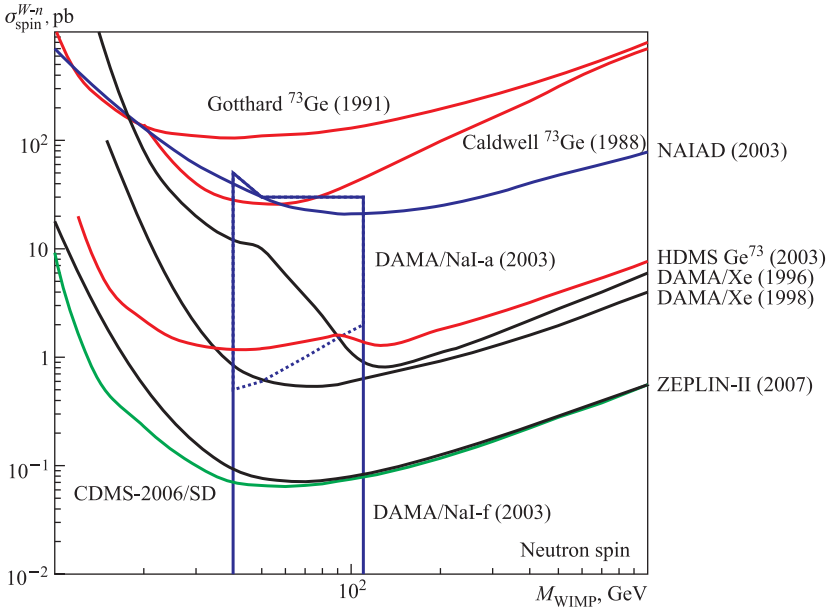

Fig. 6. Exclusion curves for the spin-dependent WIMP–neutron cross sections (σ^n_{SD} versus the WIMP mass). The DAMA/NaI-a(f) contours for the WIMP–neutron SD interaction (subdominating in ^{127}I) are obtained from the relevant figures of [45, 46]. Note that the NAIAD curve [136] here corresponds to the WIMP–neutron SD interaction subdominant for ^{127}I. The WIMP–proton SD interaction dominates for this nucleus. The curve was obtained in the approach of [115]. It is much weaker in comparison with both the DAMA/Xe and the HDMS-2003 curves. (For more details see [51] and Fig. 12)

and therefore has in principle two constraints [68] for the neutralino–proton a_p and neutralino–neutron a_n effective spin couplings, as follows from relation (5). From Eq. (5) one can also see that contrary to the SI case (4) there is, in general, no factorization of the nuclear structure for $\sigma^A_{\text{SD}}(0)$. Both proton $\langle \mathbf{S}^A_p \rangle$ and neutron $\langle \mathbf{S}^A_n \rangle$ spin contributions simultaneously enter into formula (5) for the SD WIMP–nucleus cross section $\sigma^A_{\text{SD}}(0)$. Nevertheless, for the most interesting isotopes either $\langle \mathbf{S}^A_p \rangle$ or $\langle \mathbf{S}^A_n \rangle$ dominates ($\langle \mathbf{S}^A_{n(p)} \rangle \ll \langle \mathbf{S}^A_{p(n)} \rangle$) [51, 70].

In earlier considerations [28, 94, 97, 103, 105, 111] one reasonably assumed that the nuclear spin was carried by the «odd» unpaired group of protons or neutrons and only one of either $\langle \mathbf{S}^A_n \rangle$ or $\langle \mathbf{S}^A_p \rangle$ was nonzero. In this case all possible nonzero-spin target nuclei can be classified into n-odd and p-odd groups. Following this classification, the current experimental situation for the spin-dependent WIMP–*proton* and WIMP–*neutron* cross sections is naturally presented separately in Fig. 5 and Fig. 6. The DAMA/NaI-a(f) contours for the WIMP–proton

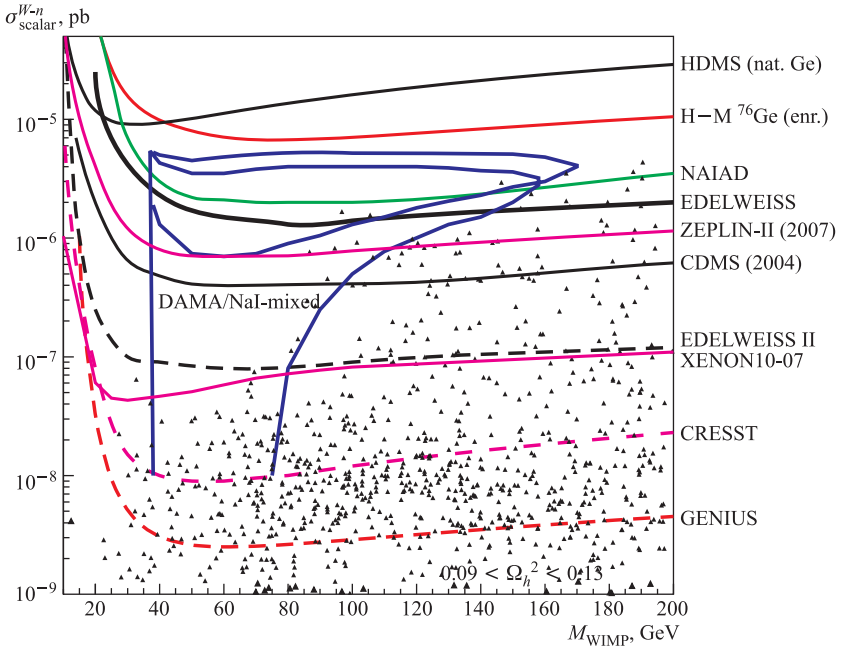

Fig. 7. WIMP–nucleon cross section ($\sigma^p_{\text{SI}}(0)$) limits in pb for spin-independent (scalar) interactions as a function of the WIMP mass in GeV. Shown are contour lines for some of the present experimental limits (solid lines) and some of projected experiments (dashed lines). All curves are obtained in the one-coupling dominance approach with $\sigma_{\text{SD}} = 0$. For example, the closed DAMA/NaI contour corresponds to complete neglection of SD WIMP–nucleon interaction. The open DAMA contour is obtained in [46] with the assumption that $\sigma_{\text{SD}} = 0.08$ pb > 0. Theoretical expectations for σ^p_{SI} in the effMSSM from [51] are also shown by scatter plots for a relic neutralino density $0.09 < \Omega_\chi h^2_0 < 0.13$ (black triangles) (see [51])

SD interaction (dominating in ^{127}I) obtained on the basis of the positive signature of the annual modulation (closed contour) [46] and within the mixed coupling framework (open contour) [45] are also presented in Fig. 5. Similarly, the DAMA/NaI-a(f) [46] contours for the WIMP–neutron SD interaction (subdominant in ^{127}I) are given in Fig. 6. There are also exclusion curves for the SD cross section from the CDMS [137] and EDELWEISS [138] experiments with natural-germanium bolometric detectors (due to the small Ge-73 admixture).

To compare experimental data with theoretical estimations in the effMSSM [51] one can superimpose the scatter plots for the SD and SI LSP–proton and LSP–neutron cross sections (from Figs. 4 or 3) in Figs. 5, 6, and 7. This is a traditional way to perform this comparison. One can easily see that both

calclulated SD LSP–proton and LSP–neutron cross sections fall below the frames of Figs. 5 and 6, respectively. In particular, this means that experimental data (avaliable at present in the form of exclusion curves) do not allow one to restrict the SUSY LSP–nucleon spin couplings. This is not the case for the SI WIMP–nucleon coupling. The scattered points (black triangles) for $\sigma^p_{\rm SI}$ calculated in the effMSSM are clearly seen in Fig. 7. Some of these points are already excluded by the DM measuremnts.

Nevertheless, one would like to note that, for example, the calculated scatter plots for $\sigma^p_{\rm SD}$ (Fig. 5) are obtained without any assumption of $\sigma^n_{\rm SD} = 0$ (and $\sigma^p_{\rm SI} = 0$), but the experimental exclusion curves for $\sigma^p_{\rm SD}$ were traditionally extracted from the data with the spin–neutron (and scalar) contribution fully neglected, i.e., under the assumption that $\sigma^n_{\rm SD} = 0$ (and $\sigma^p_{\rm SI} = 0$). This *one-spin-coupling dominance scheme* (always used before the new approaches were proposed in [115] and in [44,46,47]) gave a bit too pessimistic exclusion curves, but allowed direct and *correct* comparison of sensitivities for different DM search experiments. More stringent constraints on $\sigma^p_{\rm SD}$ can be obtained [44, 46, 47, 115] by assuming both $\sigma^p_{\rm SD} \neq 0$ and $\sigma^n_{\rm SD} \neq 0$ (although the contribution of the neutron spin is usually very small because $\langle \mathbf{S}^A_n \rangle \ll \langle \mathbf{S}^A_p \rangle$). Therefore a direct comparison of an old-fashioned exclusion curve with a new one could in principle mislead one to a wrong conclusion about better sensitivity of the new experiment.

The same conclusion on the one-coupling dominance approach to a great extent concerns [46, 47, 51, 52] the direct comparison of the *old* SI exclusion curves (obtained with $\sigma_{\rm SD} = 0$) with the *new* SI exclusion curves (obtained with $\sigma_{\rm SD} > 0$) as well as with the results of the SUSY calculations. One can see from Fig. 7 that the *new-type* DAMA/NaI open contour (when $\sigma_{\rm SD} > 0$) is in agreement with the best exclusion curves of the CDMS and EDELWEISS as well as with SUSY calculations. One knows that both of these latter experiments have natural germanium (almost purely spinless) as a target and therefore have only little sensitivity to the spin-dependent WIMP–nucleon couplings (for them $\sigma_{\rm SD} \simeq 0$). Therefore, these experiments exclude only the pure SI interpretation of the DAMA annual modulation signal [53, 54, 137, 139, 140]. The statement that this DAMA result is *completely* excluded by the results of these cryogenic experiments and is inconsistent with the SUSY interpretation (see, for example, [141]) is simply wrong (see also discussions in [54, 56, 58, 59]).

The event-by-event CDMS and EDELWEISS background discrimination (via simultaneous charge and phonon signal measurements) is certainly very important. Nevertheless, the DAMA annual signal modulation is one of a few available *positive* signatures of WIMP–nucleus interactions and the importance of its observation goes far beyond a «simple» background reduction. Therefore, to completely exclude the DAMA result, a new experiment, being sensitive to the modulation signal, would have to confirm or exclude this modulation signal on the basis of the same or much better statistics.

Furthermore, taking seriously the positive DAMA result together with the negative results of the CDMS and EDELWEISS as well as the results of [57], one can arrive at a conclusion about simultaneous existence and importance of both SD and SI WIMP–nucleus interactions.

4. MIXED SPIN–SCALAR WIMP–NUCLEON INTERACTIONS

The accurate calculations of spin nuclear structure [31,66,70,88,98,100,101, 106,108,112–114] demonstrate that contrary to the simplified odd-group approach both $\langle \mathbf{S}_p^A \rangle$ and $\langle \mathbf{S}_n^A \rangle$ differ from zero, but nevertheless one of these spin quantities always dominates ($\langle \mathbf{S}_p^A \rangle \ll \langle \mathbf{S}_n^A \rangle$, or $\langle \mathbf{S}_n^A \rangle \ll \langle \mathbf{S}_p^A \rangle$). It follows form Eq. (6) that *if together* with the dominance like $|\langle \mathbf{S}_{p(n)}^A \rangle| \ll |\langle \mathbf{S}_{n(p)}^A \rangle|$ one would have the WIMP–proton and WIMP–neutron couplings of the same order of magnitude (*not* $|a_{n(p)}| \ll |a_{p(n)}|$), the situation could look like that in the odd-group model and one could safely (at the current level of accuracy) neglect a subdominant spin contribution in the data analysis due to the inequality: $|a_p \langle \mathbf{S}_p^A \rangle| \ll |a_n \langle \mathbf{S}_n^A \rangle|$. Nevertheless, it was shown in [115] that in the general SUSY model one can meet right a case when $a_{n(p)} \ll a_{p(n)}$ and the proton and neutron spin contributions are strongly mixed, i.e., $|a_p \langle \mathbf{S}_p^A \rangle| \approx |a_n \langle \mathbf{S}_n^A \rangle|$.

To separately constrain the SD proton and neutron contributions at least two new approaches appeared in the literature [45, 115]. As the authors of [115] claimed, their method has the advantage that the limits on individual WIMP–proton and WIMP–neutron SD cross sections for a given WIMP mass can be combined to give a model-independent limit on the properties of WIMP scattering from both protons and neutrons in the target nucleus. The method relies on the assumption that the WIMP–nuclear SD cross section can be presented in the form $\sigma_{\rm SD}^A(0) = \left(\sqrt{\sigma_{\rm SD}^p|_A} \pm \sqrt{\sigma_{\rm SD}^n|_A} \right)^2$, where $\sigma_{\rm SD}^p|_A$ and $\sigma_{\rm SD}^n|_A$ are auxiliary quantities, not directly connected with measurements. Furthermore, to extract a constraint on the *subdominant* WIMP–proton spin contribution one should assume the proton contribution dominance for a nucleus whose spin is almost completely determined by the neutrons. From one side, this may look almost useless, especially because these subdominant constraints are always much weaker than the relevant constraints obtained directly with a proton-odd group target (one can compare, for example, the restrictive potential of the NAIAD exclusion curves in Figs. 5 and 6). From another side, the very large and very small ratios $\sigma_p/\sigma_n \sim |a_p|/|a_n|$ obtained in [115] correspond to neutralinos which are extremely pure gauginos. In this case, Z-boson exchange in SD interactions is absent and only sfermions give contributions to the SD cross sections. This is a very particular (fine-tuning) case which is hardly to be in agreement with the present

SUSY search experiments. Following an analogy between neutrinos and neutralinos one could assume that neutralino couplings with the neutron and the proton should not be very different and one could expect preferably $|a_n|/|a_p| \approx O(1)$. The relation $|a_n|/|a_p| \approx O(1)$ was checked in [69, 121] for large LSP masses. For relatively low LSP masses $m_\chi < 200$ GeV in effMSSM [8, 37, 116–119, 124] the a_n-to-a_p ratio is located within the bounds [51]:

$$0.5 < \left|\frac{a_n}{a_p}\right| < 0.8. \tag{23}$$

Therefore in the model the couplings are almost the same and one can safely neglect the $\langle \mathbf{S}^A_{p(n)} \rangle$-spin contribution in the analysis of the DM data for a nuclear target with $\langle \mathbf{S}^A_{p(n)} \rangle \ll \langle \mathbf{S}^A_{n(p)} \rangle$.

Furthermore, when one compares in the same figure an exclusion curve for SD WIMP–proton coupling, obtained without subdominant SD WIMP–neutron contribution and without SI contribution (all curves in Fig. 5 except the one for NAIAD [136] and the one for Tokyo-LiF [142]), with a curve from the approach of [115], when the subdominant contribution is included (the NAIAD and Tokyo-LiF curves in Fig. 5), one «*artificially*» improves the sensitivity of the *latter* curves (NAIAD or Tokyo-LiF) in comparison with the former ones. To be consistent and for reliable comparison of sensitivities of these experiments, one should, at least, coherently recalculate all previous curves in the new manner. This message was clearly stressed in [46].

The same arguments are true for the results of the SIMPLE experiment [143] and search for DM with NaF bolometers [144] where the SI contribution seems also to be completely ignored. Although ^{19}F has the best properties for investigation of WIMP–nucleon spin-dependent interactions (see, for example, [88]), it is not obvious that one should completely ignore spin-independent WIMP coupling with the fluorine. For example, in the relation $\sigma^A \sim \sigma^{A,p}_{\mathrm{SD}} \left[\frac{\sigma^A_{\mathrm{SI}}}{\sigma^{A,p}_{\mathrm{SD}}} + \left(1 + \sqrt{\frac{\sigma^{A,n}_{\mathrm{SD}}}{\sigma^{A,p}_{\mathrm{SD}}}} \right)^2 \right]$ which follows from Eqs. (4)–(6), it is not a priori clear that $\frac{\sigma^A_{\mathrm{SI}}}{\sigma^{A,p}_{\mathrm{SD}}} \ll \frac{\sigma^{A,n}_{\mathrm{SD}}}{\sigma^{A,p}_{\mathrm{SD}}}$, i.e., the SI WIMP–nucleus interaction is much weaker than the subdominant SD WIMP–nucleus one. At least for isotopes with atomic number $A > 50$ [29, 33] the neglection of the SI contribution would be a larger mistake than the neglection of the subdominant SD WIMP–neutron contribution, when the SD WIMP–proton interaction dominates.

Therefore we would like to note that the «old» odd-group-based approach to analysis of the SD data from experiments with heavy enough targets (for example, ^{73}Ge) is still quite suitable, especially when it is not obvious that (both) spin couplings dominate over the scalar one.

From measurements with ^{73}Ge one can extract, in principle, not only the dominant constraint for WIMP–nucleon coupling a_n (or $\sigma^n_{\rm SD}$) but also the constraint for the subdominant WIMP–proton coupling a_p (or $\sigma^p_{\rm SD}$) using the approach of [115]. Nevertheless, the latter constraint will be much weaker in comparison with the constraints from p-odd group nuclear targets, like ^{19}F or I. This fact is illustrated by the NAIAD (NaI, 2003) curve in Fig. 6, which corresponds to the subdominant WIMP–neutron spin contribution extracted from the p-odd nucleus ^{127}I.

Another approach for the mixed spin–scalar coupling data presentation, of Bernabei et al. [45], is based on an introduction of the so-called effective SD nucleon cross section $\sigma^{pn}_{\rm SD}(0)$ ($\sigma_{\rm SD}$ in [45,46]) and coupling mixing angle θ (see Eq. (7)) instead of $\sigma^p_{\rm SD}(0)$ and $\sigma^n_{\rm SD}(0)$. With these definitions the SD WIMP–proton and WIMP–neutron cross sections are given by relations (8).

In Fig. 8 the WIMP–nucleon spin and scalar mixed couplings allowed by the annual modulation signature from the 100-kg DAMA/NaI experiment are shown inside the shaded regions. The regions from [45, 46] in the ($\sigma_{\rm SI}$, $\sigma_{\rm SD}$) space for $40 < m_{\rm WIMP} < 110$ GeV cover spin–scalar mixing coupling for the proton ($\theta = 0$ case of [45,46], Fig. 8, *a*) and spin–scalar mixing coupling for the neutron ($\theta = \pi/2$, Fig. 8, *b*). From nuclear physics one has for the proton spin dominated

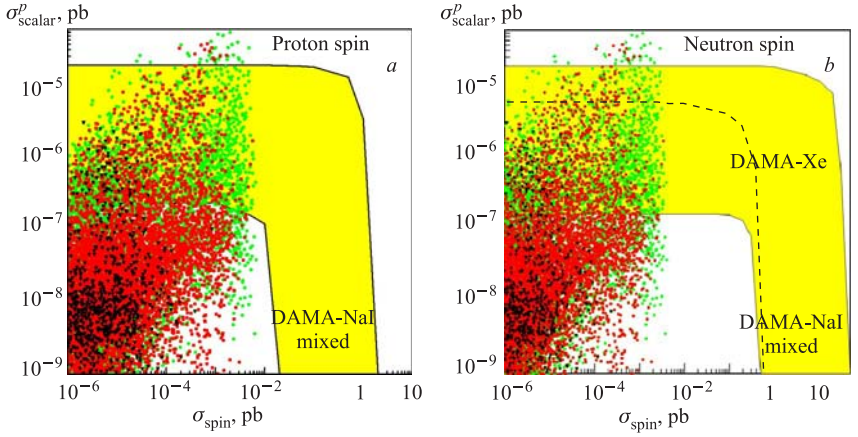

Fig. 8. The DAMA-NaI allowed region from the WIMP annual modulation signature in the ($\xi\sigma_{\rm SI}$, $\xi\sigma_{\rm SD}$) space for $40 < m_{\rm WIMP} < 110$ GeV [45, 46]. Plot *a* corresponds to the dominating (in ^{127}I) SD WIMP–proton coupling alone ($\theta = 0$) and the plot *b* corresponds to the subdominating SD WIMP–neutron coupling alone ($\theta = \pi/2$). The scatter plots give correlations between $\sigma^p_{\rm SI}$ and $\sigma_{\rm SD}$ in the effMSSM ($\xi = 1$ is assumed) for $m_\chi < 200$ GeV [51]. In plot *b* also the DAMA liquid xenon exclusion curve from [45] is given (dashed line). From [51]

^{23}Na and ^{127}I $\langle \mathbf{S}_n \rangle / \langle \mathbf{S}_p \rangle < 0.1$ and $\langle \mathbf{S}_n \rangle / \langle \mathbf{S}_p \rangle < 0.02{-}0.23$, respectively. For $\theta = 0$ due to the p-oddness of the I target, the DAMA WIMP–proton spin constraint is the most severe one (see Fig. 5). In the Fig. 8, *b* we also present the exclusion curve (dashed line) for the WIMP–proton spin coupling from the proton-odd isotope ^{129}Xe obtained under the mixed coupling assumptions [45] from the DAMA-LiXe (1998) experiment [145–147]. For the DAMA NaI detector the $\theta = \pi/2$ means no $\langle \mathbf{S}_p \rangle$ contribution at all. Therefore, in this case DAMA gives the subdominant $\langle \mathbf{S}_n \rangle$ contribution only, which could be compared further with the dominant $\langle \mathbf{S}_n \rangle$ contribution in ^{73}Ge. The scatter plots in Fig. 8 give σ^p_{SI} as a function of σ^p_{SD} (Fig. *a*) and σ^n_{SD} (Fig. *b*) calculated in the effMSSM with parameters from Eq. (22) under the same constraints on the relic neutralino density as in Fig. 4 [51]. Filled circles correspond to relic neutralino density $0.0 < \Omega_\chi h^2_0 < 1.0$, squares correspond to subdominant relic neutralino contribution $0.002 < \Omega_\chi h^2_0 < 0.1$ and black triangles correspond to the WMAP density constraint $0.094 < \Omega_\chi h^2_0 < 0.129$ [18, 19].

The constraints on the SUSY parameter space in the mixed coupling framework in Fig. 8 look, in general, much stronger in comparison with the traditional approach based on the one-coupling dominance. It follows from Fig. 8 that when the LSP is the subdominant DM particle (squares in the figure), SD WIMP–proton and WIMP–neutron cross sections at a level of $(3{-}5) \cdot 10^{-3}$ pb are allowed, but the WMAP relic density constraint (triangles) together with the DAMA restrictions leaves only $\sigma^{p,n}_{\mathrm{SD}} < 3 \cdot 10^{-5}$ pb without any visible reduction of allowed values for σ^p_{SI}. In general, according to the DAMA restrictions, very small SI cross sections are completely excluded, only $\sigma^p_{\mathrm{SI}} > (3{-}5) \cdot 10^{-7}$ pb are allowed. The SD cross section is not yet restricted at all. It is seen that for the allowed values of the SI contribution the SD DAMA sensitivity did not yet reach the upper bound for the SD LSP–proton cross section of $5 \cdot 10^{-2}$ pb calculated for the nucleon spin structure from [148].

In general, the famous DAMA «conflict» with the other (negative) DM results can be safely bypassed on the basis of the above-mentioned mixed spin–scalar coupling approach, where both SD and SI couplings are considered simultaneously as non-negligible.

5. THE MIXED COUPLING APPROACH FOR THE HIGH-SPIN ^{73}Ge

In this Section, on the basis of the high-spin ^{73}Ge detector HDMS [91, 92], the mixed spin–scalar coupling approach is used *to demonstrate how one can significantly improve* the quality of the exclusion curves in comparison with the one-coupling dominance result of [79].

The Heidelberg Dark Matter Search (HDMS) experiment used a special configuration of two Ge detectors to efficiently reduce the background (due to anti-

coincidence of inner and outer detectors) [79, 91, 92]. A small, p-type Ge crystal (enriched by 86% in ^{73}Ge) is surrounded by a well-type natural Ge crystal, both being mounted into a common cryostat system (see Fig. 9, *a* for a schematic view). The HDMS with enriched ^{73}Ge inner detector was the first and till now unique setup with a high-spin ($J = 9/2$) Ge target isotope for direct DM search. The main idea of the new combined analysis relies on the unique possibility that two different isotope targets (from natural Ge and enriched ^{73}Ge) were used as inner detector in the same HDMS setup under the same outer background conditions of LNGS.

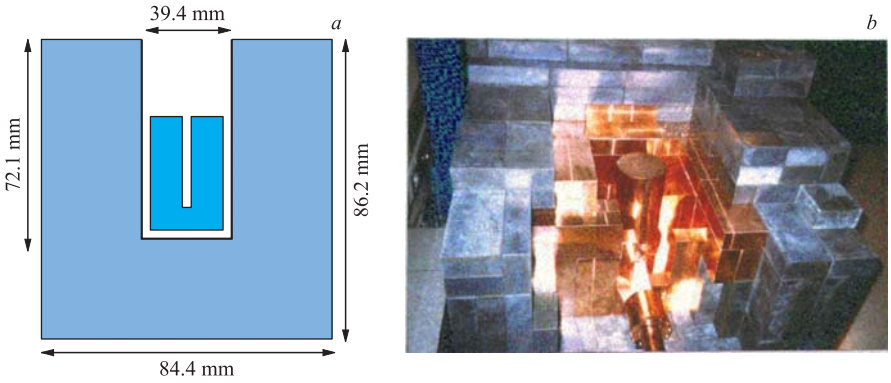

Fig. 9. *a*) Schematic view of the HDMS detector configuration. A small Ge crystal is surrounded by a well-type Ge crystal, the anticoincidence between them is used to suppress background created by external photons. *b*) The HDMS detector in its open shield during the installation in the Gran Sasso Underground Laboratory. The inner shield is made of 10 cm electrolytic copper, the outer one of 20 cm Boliden lead [92, 149]

In fact, the first simple estimation of the prospects for DM search and SUSY constraints with the high-spin ^{73}Ge detector HDMS assuming mixing of WIMP–neutron spin and WIMP–nucleon scalar couplings together with available results from the DAMA-NaI and LiXe experiments [44, 46, 47, 145–147] was performed in [51]. Furthermore, recently in the mixed spin–scalar coupling approach the data from *both* HDMS experiments with *natural* Ge and with *enriched* ^{73}Ge were *simultaneously* re-analyzed. This new analysis together with a new procedure for background identification and subtraction from the measured ^{73}Ge spectrum allowed one to obtain a significant (about one order of magnitude) improvement for the limits on the WIMP–neutron spin-dependent coupling. As a result, the HDMS experiment is now giving the most sensitive limits on the WIMP–neutron spin coupling for WIMP masses larger than 60–65 GeV/c^2 [93].

The evaluation of the DM limits (exclusion curves) on the WIMP–nucleon SD or SI cross sections follows, in general (see, for example, [91, 150, 151]),

the conservative assumption that the whole experimentally measured spectrum is saturated by the WIMP-induced events. Consequently, any excess events from the calculated spectrum above the relevant experimental spectra in any energy interval are considered as forbidden (at a given confidence level). In our case we assume that for any given WIMP mass m_χ both $\sigma_{\rm SI} \equiv \sigma_{\rm SI}(m_\chi)$ and $\sigma_{\rm SD} \equiv \sigma_{\rm SD}(m_\chi)$ WIMP–nucleon interaction cross sections are excluded if

$$\frac{dR(E_R)}{dE_R} = \kappa_{\rm SI}(E_R, m_\chi)\,\sigma_{\rm SI} + \kappa_{\rm SD}(E_R, m_\chi)\,\sigma_{\rm SD} > \frac{dR^{\rm data}}{dE_R}(\epsilon, E_R) \equiv \equiv R^{\rm data}(\epsilon, E_R), \quad (24)$$

or both upper limit values for $\sigma_{\rm SI}$ and $\sigma_{\rm SD}$ can be obtained as solutions of the following equation:

$$\kappa_{\rm SI}(E_R, m_\chi)\,\sigma_{\rm SI} + \kappa_{\rm SD}(E_R, m_\chi)\,\sigma_{\rm SD} = R^{\rm data}(\epsilon, E_R)$$

for all available recoil energies E_R above the threshold energy ϵ. The notations are given by Eqs. (7), (8), (15), and (16). The subdominant contribution from WIMP–proton spin coupling proportional to $\langle \mathbf{S}_p^A \rangle$ can be safely neglected for ^{73}Ge. The ^{73}Ge isotope looks with a good accuracy like an almost pure neutron–odd group nucleus with $\langle \mathbf{S}_n \rangle \gg \langle \mathbf{S}_p \rangle$ (Table 2). Therefore in our consideration $\sigma_{\rm SD} \equiv \sigma_{\rm SD}^n$ and $\cos\theta = 0$. For the WIMP mass density in our Galaxy the value $\rho_\chi = 0.3$ GeV/cm^3 is used.

To find both $\sigma_{\rm SI}$ and $\sigma_{\rm SD}$, for any given m_χ, in accordance with Eq. (24) the following functional

$$\chi^2(m_\chi, \epsilon) = \\ = \sum_j^{\rm spectra} \sum_i^{\rm bin} \frac{\left(R^j(\epsilon, E_i) - \kappa_{\rm SI}(E_i, m_\chi)\,\sigma_{\rm SI} - \kappa_{\rm SD}^j(E_i, m_\chi)\,\sigma_{\rm SD}\right)^2}{(\Delta R^j(E_i))^2} \quad (25)$$

can be numerically minimized, where $R^j(E_i)$ and $\Delta R^j(E_i)$ are measured rate and its error (in counts/day/kg/keV) in ith energy bin for jth used spectrum ($j = 1, 2$ for natural Ge and ^{73}Ge). The two main used spectra are given in Fig. 10. Only the «cleanest» background spectrum with the ^{73}Ge target collected in the latest runs of the experiment (with numbers 721–1000) was used in the analysis (histogram on Fig. 10, *b*). For both spectra the visual energy threshold $\epsilon = 4$ keV is used.

Comparing both the «most accurate» (runs 721–1000 in Fig. 10, *b*) HDMS ^{73}Ge spectrum and the natural Ge spectrum one can see obviously some nonvanishing *extra* background contribution in the first spectrum relative to the second one. In general, such a possibility is not new. The improvement in the exclusion

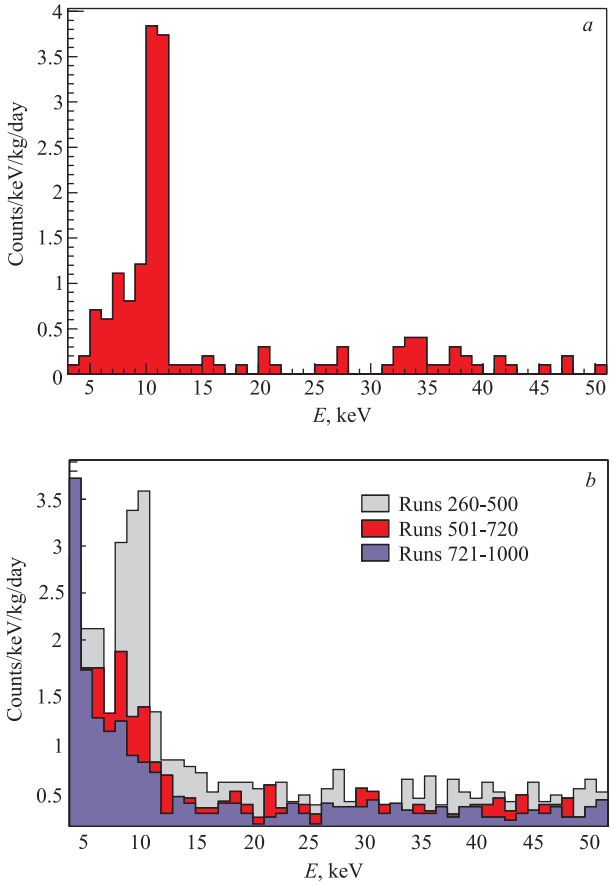

Fig. 10. HDMS spectra used in the analysis. *a*) Spectrum obtained in the first prototype phase of the HDMS experiment with the inner detector from natural Ge (exposure 9.9 kg/day [150]. *b*) Spectrum obtained from the full HDMS setup with the inner detector from enriched ^{73}Ge (exposure 85.5 kg/day) [79]. It is separated in 3 sets of runs of 30.9, 29.5 and 27.6 kg/day, respectively. The histogram corresponds to the latest (most clean) runs 721–1000. From [79]

curves by taking into account known sources of background during DM searches with Ge detectors was demonstrated, for example, in [152] and further discussed in [153]. Therefore for this HDMS ^{73}Ge spectrum we allow the possibility to fit simultaneously with the SD and SI cross sections some constant (as a function of the recoil energy) background contribution, too. The effect of this extra background contribution is discussed later on.

For a semiconductor germanium detector one has to take into account the ionization efficiency. For the HDMS Ge setup in the (visual) energy interval $4 < E_R < 50$ keV a simple relation between the visible recoil energy and the real recoil energy — $E_{\rm vis} \equiv E_R = 0.14 E^{1.19}_{\rm real\ recoil} \approx Q E_{\rm real\ recoil}$ — can be used with $Q = 0.33$ being the quenching factor for Ge [79, 91, 150, 151].

One can note that for any WIMP mass, m_χ, and any target mass, M_A, due to kinematics one has not to expect any WIMP-induced event at all with

$$E_R > E_R^{\max} = Q \frac{2 v_{\max}^2 M_A m_\chi^2}{(M_A + m_\chi)^2} = Q \frac{2 v_{\max}^2}{M_A} \mu_A^2, \qquad v_{\max} \approx v_{\rm esc}. \tag{26}$$

For example, $E_R^{\max} = 4\ (50)$ keV, for a Ge detector and $m_\chi = 12\ (77)$ GeV/c^2. It is clear from Eq. (26) that for fixed $v_{\max}$, M_A and the detector energy threshold ϵ there are undetectable WIMPs (with rather light m_χ) if the maximal recoil energy, they can produce, is smaller than the threshold: $E_R^{\max} < \epsilon$. Therefore one has two restrictions for the theoretical event rate as a function of the WIMP mass m_χ:

$$R(E_R > E_R^{\max}(m_\chi)) \equiv 0 \quad \text{and} \quad R(E_R^{\max}(m_\chi) < \epsilon) \equiv 0. \tag{27}$$

The first one allows background (for the WIMP–nucleus signal) estimation in the ^{73}Ge measured spectrum, which could lead to a remarkable improvement of the deduced exclusion curves.

Now we turn to our main analysis of both HDMS spectra in the mixed spin–scalar coupling approach and extract limits for both cross sections $\sigma_{\rm SI}$ and $\sigma_{\rm SD}$ simultaneously using formulas (24), (25). To obtain from the available data the most accurate exclusion curve one can use two minimization approaches. The first (main) approach relied on indeed direct simultaneous determination of the SD and SI WIMP–nucleon limits for a given WIMP mass m_χ (exclusion curves for $\sigma_{\rm SD}(m_\chi)$ and $\sigma_{\rm SI}(m_\chi)$) by means of minimization of the discrepancy between our calculated estimations of the expected rates and both above-mentioned experimental spectra. In our second (auxiliary) approach assuming SI coupling dominance ($\sigma_{\rm SD} = 0$), we first extracted only the SI WIMP–nucleon limit $\sigma_{\rm SI}(m_\chi)$ from the natural Ge spectrum (Fig. 10, *a*). Next, for each WIMP mass and above defined $\sigma_{\rm SI}(m_\chi)$ we extracted only the SD WIMP–nucleon limit $\sigma_{\rm SI}(m_\chi)$ from the cleanest background spectrum with ^{73}Ge (Runs 721–1000, 27.6 kg/day spectrum in Fig. 10, *b*). In both cases the obtained results are rather similar.

Furthermore trying to improve the quality of the exclusion curves one can use a sliding variable energy window to check the excess events above the experimental spectrum (in these energy window intervals) as used in previous papers [79, 91, 92, 150]. The minimum among the cross-section values obtained via the multiple fits is taken as the cross section for the corresponding WIMP mass. We used 5-keV minimal width of this energy window as in [150, 151] and a 10-keV window as well.

First, the possible improvements of the exclusion curves due to variation of minimization conditions, used in the data analysis, were studied. The relevant exclusion curves obtained from the *simultaneous* analysis of *both* HDMS spectra within the mixed spin–scalar coupling approach are given in Fig. 11 as a function of the WIMP mass.

Figure 11, *a* shows the upper limits for the spin-independent WIMP–nucleon cross section $\sigma_{\rm SI}$ as a function of WIMP mass obtained under different minimization conditions. Figure 11, *b* shows the upper limits for the spin-dependent

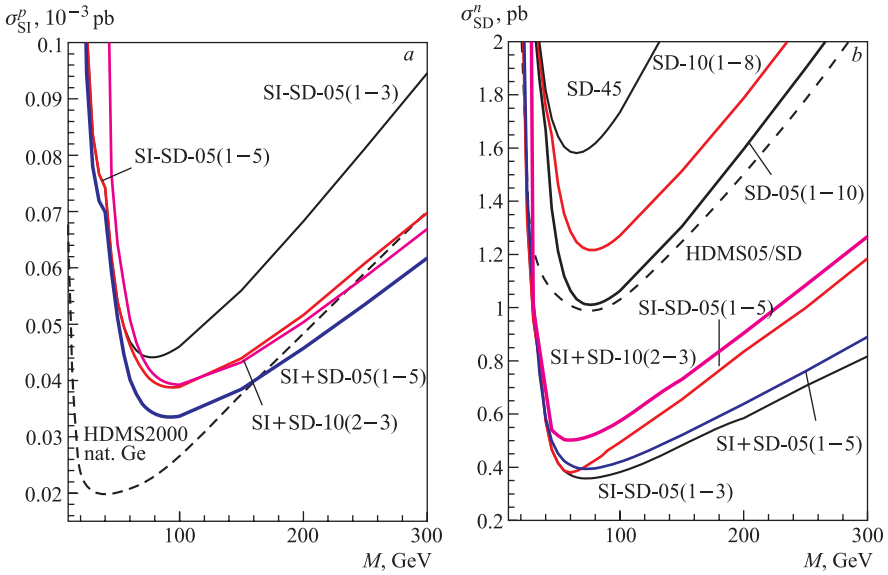

Fig. 11. Spin-independent $\sigma_{\rm SI}$ (*a*) and spin-dependent $\sigma_{\rm SD}$ (*b*) cross section upper limits as a function of WIMP mass (exclusion curves) obtained from *simultaneous* analysis of both HDMS Ge spectra under different minimization conditions. The label «SI-SD-05(1–5)» means that *only* the spectrum from natural Ge (Fig. 10, *a*) is used first to extract a SI limit (auxiliary approach) using 5-keV sliding window and taking into account only the first 5 lowest energy windows to obtain the limits. Curves labeled with «SD + SI-05(1-5)» are obtained from indeed *simultaneous* minimization of both natural Ge and the best (Fig. 10, *b*) enriched ^{73}Ge spectra using the 5-keV sliding window and only the first 5 lowest energy windows. The label «SI + SD-10(2–3)» denotes the same procedure, but with 10-keV sliding window and with the 2nd and the 3rd lowest energy windows. The other labels have analogous meaning. Dashed lines correspond to some other analyses and are given for comparison («HDMS2000, nat. Ge» from [150], «HDMS05/SD» from [79]). The thin exclusion curves «SD-45», «SD-10(1–8)», and «SD-05(1–10)» are obtained from the traditional one-coupling dominance fit of the enriched ^{73}Ge spectrum *only* and are given to illustrate the role of the sliding window width as well as the consistency with the previous result of [79]

WIMP–neutron cross section $\sigma_{\rm SD}$ (in our approximation $\sigma_{\rm SD} \equiv \sigma^n_{\rm SD}$) as a function of WIMP mass which correspond to the above-mentioned $\sigma_{\rm SI}$ limits from the plot *a*. For example, the exclusion curve labeled with «SI-SD-05(1–5)» presents in plot *a* the SI limits $\sigma_{\rm SI}(m_\chi)$ extracted *only* from the natural Ge spectrum (Fig. 10, *a*) with 5-keV sliding windows within only the first 5 lowest energy windows and under the assumption $\sigma_{\rm SD} = 0$. The relevant «SI-SD-05(1–5)» exclusion curve in plot *b* shows *correlated* SD limits $\sigma_{\rm SD}(m_\chi)$ extracted from the best enriched ^{73}Ge spectrum (Runs 721–1000, spectrum in Fig. 10, *b*) when $\sigma_{\rm SI} = \sigma_{\rm SI}(m_\chi) \neq 0$ from plot *a*. The curves labeled with «SD + SI-05(1–5)» are obtained from simultaneous minimization of both above-mentioned spectra from Fig. 10 using the 5-keV sliding window and the first 5 lowest energy windows. The other exclusion curves (with labels «SD + SI-10(2–3)» and «SD-SI-05(1–3)») are given in Fig. 11 to illustrate the exclusion curve dependence on the width of the sliding window and optimal (or nonoptimal) choice of minimization regions.

The dashed lines correspond to some other analyses and are given for comparison («HDMS2000, nat. Ge» from [150], «HDMS05/SD» from [79]). The thin exclusion curves «SD-45», «SD-10(1–8)» and «SD-05(1–10)» are obtained from the traditional one-coupling dominance fit of the enriched ^{73}Ge spectrum only and are given also to illustrate the role of the width of the sliding window as well as the consistency with the previous result of [79]. The small discrepancy between the «HDMS05/SD» and «SD-05(1–10)» curves for low WIMP masses is mainly due to our restrictions (27).

The pair of SI and SD exclusion curves with label «SD + SI-05(1–5)» corresponds to the optimal parameters of the fitting procedure and presents the best correlated exclusion curves obtained from simultaneous minimization of both spectra from natural Ge spectrum and the «cleanest» enriched ^{73}Ge spectrum. The pair has the best SI exclusion curve (plot *a*) simultaneously with almost the best SD exclusion curve (plot *b*). The visible difference between the best SI curve «SD + SI-05(1–5)» and the «HDMS2000, nat. Ge» curve from [150] is due to restrictions (27) and another energy threshold (see below) used in our analysis.

Therefore, from Fig. 11, *b* one can conclude that the most sensitive exclusion curves for the WIMP–*neutron* spin interaction («SI-SD-05(1–3)», and «SI + SD-05(1–5)») improve the relevant one-coupling dominance limit of «HDMS05/SD» [79] within a factor of 2–3 depending on the WIMP mass. This is a clear result of the mixed spin–scalar approach.

Now we consider two other possibilities to improve the quality of the exclusion curves extracted from both Ge spectra within the mixed coupling scheme. The first one is a lower recoil (visible) energy threshold for the natural Ge detector of HDMS setup. The second one is a new procedure of background subtraction from the *measured spectrum* of the ^{73}Ge isotope. This procedure *strongly* relies on the existence of a really measured spectrum.

In Fig. 12, *b* the thin exclusion curve labeled with «SD only fit» is the result of the one coupling dominance analysis of the enriched ^{73}Ge spectrum only. It repeats the relevant curve (labeled with «SD-05(1–10)») from Fig. 11. As mentioned before, the curve is consistent with the previous analysis of [79], given here with curve «HDMS05/SD».

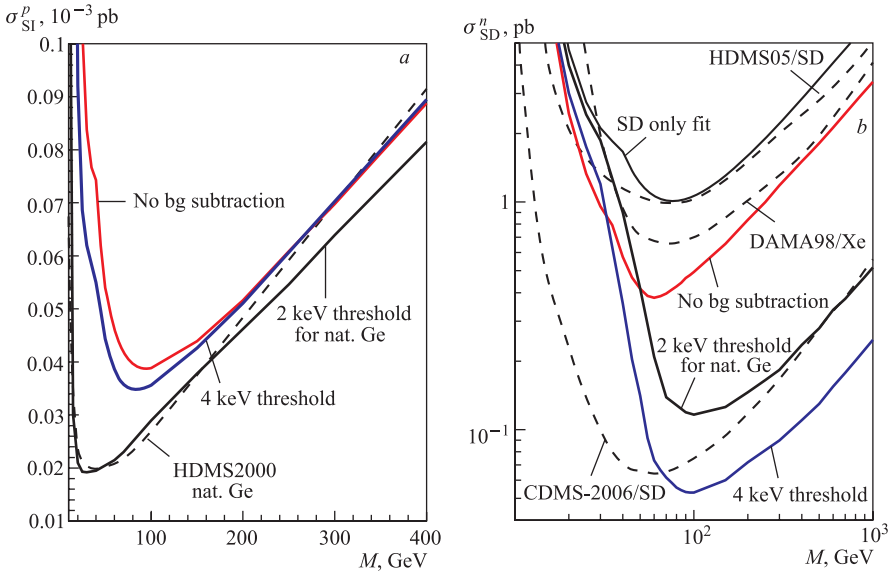

Fig. 12. Exclusion curves from *simultaneous* fit of the data from both HDMS setups. *a*) Spin-independent cross section upper limits $\sigma_{\rm SI}$ in pb as a function of WIMP mass in GeV. *b*) Spin-dependent cross section upper limits $\sigma_{\rm SD}$ as a function of WIMP mass which correspond to the $\sigma_{\rm SI}$ limits from the left panel. The label «No bg subtraction» shows the best exclusion curves obtained from simultaneous minimization of both natural Ge (Fig. 10, *a*) and the best (Runs 721–1000, spectrum in Fig. 10, *b*) enriched ^{73}Ge spectra within mixed spin–scalar coupling approach *without* any background subtraction from the ^{73}Ge spectra. Curves labeled with «4 keV threshold» are from the same simultaneous minimization of both natural Ge and the best enriched ^{73}Ge spectra but with extra background of 0.11 events/kg/day extracted from the ^{73}Ge spectrum. The curves labeled with «2 keV threshold for nat. Ge» are from the same procedure as above, but when threshold for the natural Ge spectrum is equal to 2 keV. The dashed curve reproduces the best HDMS SI limits from [150] given here as «HDMS2000, nat. Ge». The thin exclusion curve «SD only fit» from the traditional one-coupling dominance fit of the enriched ^{73}Ge spectrum only is given for comparison with the previous analysis of [79] labeled with «HDMS05/SD». The best exclusion dashed curve for WIMP–neutron spin coupling from CDMS Collaboration [154] is labeled with «CDMS-2006/SD». The last dashed line «DAMA98/Xe» corresponds to DAMA results from [146]. Another comparative result from ZEPLIN-I [155] (not shown) is located above the CDMS curve nearby the black one

The curves labeled with «No bg subtraction» repeat here the best exclusion curves («SI + SD-05(1–5)» in Fig. 11) obtained within the mixed spin–scalar coupling approach from simultaneous analysis of both natural Ge and the best enriched ^{73}Ge spectra. The same recoil energy threshold of 4 keV was taken for both Ge spectra. This threshold corresponds to the real threshold of the HDMS final setup with enriched ^{73}Ge [91].

We reproduce in Fig. 12 both exclusion curves «SD only fit» and «No bg subtraction» (from Fig. 11) for our further consideration and with the aim to clearly demonstrate again that the most sensitive HDMS exclusion curve («No bg subtraction») for the WIMP–*neutron* spin interaction improves the relevant one-coupling dominance limit of «HDMS05/SD» [79] and the «SD only fit» curve within a factor of 2–3.

We stress that this «No bg subtraction» curve is *obtained from the raw HDMS data without any active or passive background substraction*.

The visible difference at low WIMP masses between SI exclusion curve «No bg subtraction» and the «HDMS2000, nat. Ge» curve from [150] (in Fig. 12, *b*) is mainly due to the lower recoil energy threshold of 2 keV used in [150] for the natural Ge detector. The curve «2 keV threshold for nat. Ge» (Fig. 12, *b*) obtained indeed with a 2 keV energy threshold for the spectrum of natural Ge proves the reason of the difference.

Furthermore, the real measured spectrum of enriched ^{73}Ge (Runs 721–1000, spectrum in Fig. 10, *b*) and the first relation (27) allow one to estimate some number of counts in the spectrum which cannot be produced by means of any WIMP–nucleus interaction. In accordance with (27) for any m_χ, fixed $v_{\max}$ and M_A there is a maximal recoil energy $E_R^{\max}(m_\chi)$ (26) for which WIMP–nucleus interactions are unable to produce any signal if $E_R > E_R^{\max}(m_\chi)$ (i.e., when the measured recoil energy is larger than the maximally possible recoil energy for a given WIMP mass). Therefore, for fixed m_χ the measured recoil spectrum in the region $E_R > E_R^{\max}(m_\chi)$ is directly some background which can be approximated, for example, as a constant function of the recoil energy, independent of m_χ. One can estimate these background constants for each allowed m_χ (still $E_R^{\max}(m_\chi) < 50$ keV) and assume the minimal of these constants (0.11 events/kg/day/keV) to be the mean background for all measured E_R and all m_χ. Physically this extra background is completely independent of any WIMPs, therefore, being estimated for rather small $m_\chi < 100$ GeV, it can be used for all WIMP masses as well.

Therefore, with common energy threshold of 4 keV, the simultaneous minimization of both natural Ge and the best ^{73}Ge spectra *with* the above-mentioned extra background of 0.11 events/kg/day has supplied us with the pair of SD and SI exclusion curves, labeled with «4 keV threshold» in Fig. 12. This SD curve improves (at least for $m_\chi > 60$ GeV) currently the best exclusion curve (labeled with «CDMS-2006/SD») for the WIMP–neutron spin coupling from the

CDMS Collaboration [154]. The other dashed lines correspond to some other analyses and are given for comparison («HDMS2000, nat. Ge» from [150], «HDMS05/SD» from [79], and «DAMA98/Xe» from [146]).

The curves (Fig. 12, *b*) labeled with «2 keV threshold for nat. Ge» are from the same fit procedure with the extra background, but when the threshold for the natural Ge spectrum is equal to 2 keV. In this case, as mentioned above, one reproduces the best HDMS SI limits «HDMS2000, nat. Ge» from [150]. As is seen, the background subtraction from the ^{73}Ge spectrum only very weakly affects the corresponding SI curves in Fig. 12, *b*.

The main results of the analysis performed in the mixed spin–scalar coupling approach are the (correlated) limits for the cross sections σ_{SI} and σ_{SD}. Indeed, despite the traditional form of presentation of the SD and SI exclusion curves in Fig. 12 as a function of WIMP mass, one should keep in mind that these σ_{SI} and σ^n_{SD} constraints for fixed WIMP mass are strongly correlated. This correlation is presented explicitly in Fig. 13, where the dependence on WIMP mass is given indirectly by means of the points running over the curves and marked with relevant

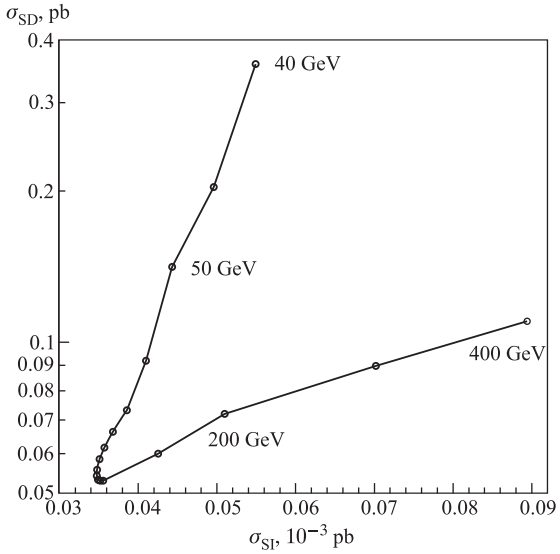

Fig. 13. Correlated spin-dependent cross section upper limit σ_{SD} and spin-independent cross section upper limit σ_{SI} obtained from the simultaneous analysis of the data from both HDMS setups. Points running over the curves mark the relevant WIMP mass values. For example, the point marked with label «200 GeV» shows the best simultaneous upper limits for SD and SI WIMP–nucleon interaction cross sections for WIMP mass 200 GeV/c^2. For the first time similar plots were given in [45]. From [93]

WIMP mass values. For example, the point marked with label «200 GeV» shows the simultaneous upper limits for SI and SD WIMP–nucleon interaction cross sections $\sigma_{\rm SI}$ and $\sigma^n_{\rm SD}$ for $m_\chi = 200$ GeV$/c^2$. This, in principle, gives one a new requirement (for a SUSY-like theory) that for any fixed WIMP mass m_χ one should have $\sigma_{\rm SI}(\text{theor.}) \leqslant \sigma_{\rm SI}(\text{fitted})$ and $\sigma^n_{\rm SD}(\text{theor.}) \leqslant \sigma^n_{\rm SD}(\text{fitted})$ *simultaneously*.

For the sake of completeness one can compare the limits obtained (in the spin–scalar mixed coupling approach) from the HDMS experiments on the SD and SI WIMP–nucleon interaction with the relevant constraints extracted by the DAMA Collaboration from measurement of the annual signal modulation with NaI target [46]. Following the DAMA positive evidence one can accept that the most preferred interval of the WIMP mass is $40 < m_{\rm WIMP} < 110$ GeV/c^2. Other consequences of the fact one can find in [51, 52].

In Fig. 14 the new HDMS-2006 limits on the SD and SI WIMP–nucleon interactions are compared with the relevant DAMA constraints extracted from measurement of the annual signal modulation with a NaI target [46] as well as with calculation in the low-energy effective MSSM [51].

To perform the comparison with the DAMA allowed region of $\sigma_{\rm SI}$ and $\sigma^n_{\rm SD}$ (Fig. 14) only one WIMP mass $m_\chi = 80$ GeV$/c^2$ (the star in the figure) was chosen for illustration. The upper limits for all other WIMP masses, $40 < m_\chi < 110$ GeV/c^2, are *very close* to this point. The point marked with the star gives our simultaneous upper limits for $\sigma_{\rm SI}$ and $\sigma^n_{\rm SD}$ for $m_\chi = 80$ GeV/c^2. For this WIMP mass, values of $\sigma_{\rm SI}$ located above the horizontal line and of $\sigma^n_{\rm SD}$ located to the right side of the vertical line are excluded. Therefore, for any fixed WIMP mass in the domain $40 < m_\chi < 110$ GeV/c^2, SUSY-like calculations should give simultaneously $\sigma_{\rm SI}$ below the relevant (to the fixed WIMP mass) horizontal line and $\sigma^n_{\rm SD}$ to the left side of the relevant vertical line, respectively. These limits improve the DAMA-Xe limit significantly (about one order of magnitude) and exclude a DAMA allowed region of large spin-dependent WIMP–neutron cross sections.

Here, perhaps, is the right place to make another remark concerning the possibility of comparing results from DM search experiments with passive background reduction (like DAMA, HDMS, etc.) and experiments with (mostly) active background reduction (like CDMS, EDELWEISS, etc.). First, we note, that obviously any extra positively defined background-like contribution to the spectra will decrease the extracted (upper limit) values of the SD and SI cross section. Next, within the passive background reduction scheme the measured spectrum is not affected by hard- or software influence during the data taking. Extra further background reduction can be done off-line on the basis of careful investigation of the spectrum itself or, for example, with the help of pulse shape analysis. In this case the extracted background contribution is under control and well defined. On the other side, within the active background reduction approach the measured

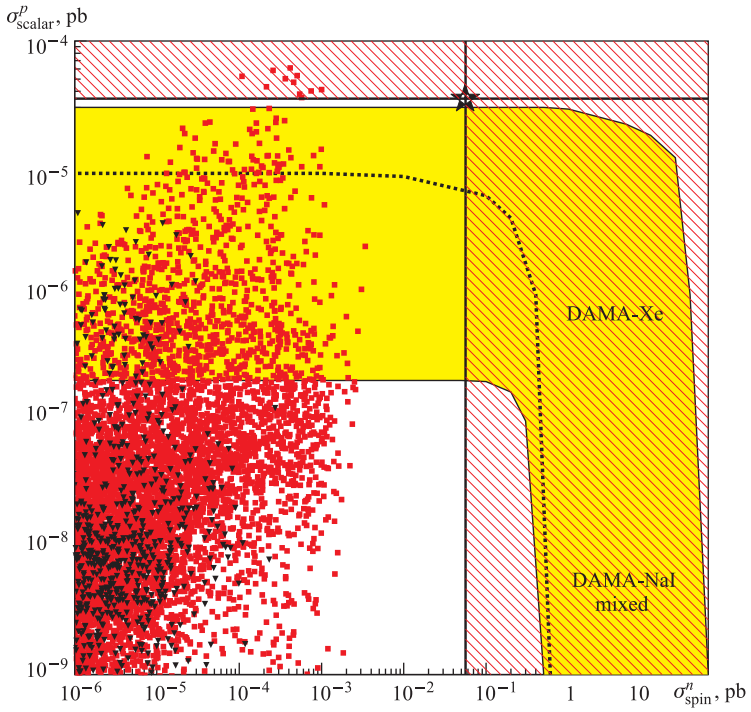

Fig. 14. The DAMA-NaI allowed region (inside the band) for SD WIMP–neutron coupling versus SI WIMP–nucleon coupling is from [46] and corresponds to $40 < m_\chi < 110$ GeV/c^2. The scatter plots from [51] give correlations between $\sigma^p_{\rm SI}$ and $\sigma^n_{\rm SD}$ in the effMSSM for $m_\chi < 200$ GeV. The squares correspond to subdominant relic neutralino contribution $0.002 < \Omega_\chi h_0^2 < 0.1$ and triangles correspond to WMAP relic neutralino density $0.094 < \Omega_\chi h_0^2 < 0.129$. The dashed line from [45] shows the DAMA-LiXe (1998) exclusion curve for $m_\chi = 50$ GeV/c^2. The star gives our simultaneous upper limits from the HDMS experiment [93] for $\sigma_{\rm SI}$ and $\sigma^n_{\rm SD}$ for $m_\chi = 80$ GeV/c^2. Therefore values of $\sigma_{\rm SI}$ above the horizontal line and of $\sigma^n_{\rm SD}$ located right from the vertical line are excluded by our analysis

spectrum already contains results of this active reduction influence on the data taking process. In this case it is not simple to hold under control the real level of extracted on-line background contribution which easily can be overestimated (see, for example, the recent discussion of the ZEPLIN-I sensitivity in [156]). Therefore, due to this obvious difference a direct comparison of exclusion curves from experiments with passive and active background reductions could be, in principle, rather misleading.

6. DISCUSSIONS

The problem of the dark matter in the Universe is a challenge for modern physics and experimental technology. To solve the problem, i.e., *at least* to detect dark matter particles, one simultaneously needs to apply the front-end knowledge of modern particle physics, astrophysics, cosmology and nuclear physics as well as one should develop, and use over long time extremely high-sensitive experimental setups, and complex data analysis methods.

Weakly interacting massive particles (WIMPs) nowadays are among the best motivated nonbaryonic dark matter candidates. In particular the lightest neutral supersymmetric particle (LSP), the neutralino, is a very good WIMP candidate. The motivation for supersymmetry arises naturally in modern theories of particle physics.

To estimate the expected direct detection rate for these WIMPs any SUSY-like model, for example, an effective low-energy minimal supersymmetric extension of the Standard Model (effMSSM), or some measured data, for example, from the DAMA experiment [157], can be used. On this basis the WIMP–proton and WIMP–neutron spin and scalar cross sections at zero-momentum transfer ($\sigma^{p,n}_{\mathrm{SD}}(0)$ and $\sigma^{p,n}_{\mathrm{SI}}(0)$) can be calculated. These calculations one usually compares with measurements, which (with the only exception of the DAMA result) are presented in the form of exclusion curves — upper limits of cross section as functions of the WIMP mass. In the case of nonobservation of any DM signal an exclusion curve simply reflects the sensitivity of a given direct DM search experiment and potentially allows one to constrain some version of SUSY-like theory, *if the curve is sensitive enough*. Therefore, the best exclusion curve is currently a clear aim of almost all dark matter search experiments (DAMA, LIBRA, and GENIUS perhaps are/were the only exceptions). The main competition between the experiments runs in the field of these exclusion curves.

Before 2000, all exclusion curves were evaluated mainly in the one-coupling dominance approach (when only one cross section was defined from the measured spectra for fixed WIMP mass), which gave slightly pessimistic (for spin-nonzero target experiments), but universal limits for all experiments. One would say that the competition between DM experiments was honest. The predictions from SUSY-like models were in general far from being reached by the data.

Mainly after the paper [115] was published in 2000 (and as well after the DAMA evidence [46]) a new kind of exclusion curves appeared. In particular, for the first time these curves were obtained for the spin-dependent WIMP–nucleon cross section limits when nonzero subdominant spin WIMP–nucleon contributions were taken into account [136, 142]. This procedure obviously improved the quality of the exclusion curves. Therefore a direct comparison of an old-fashioned exclusion curve with a new one could in principle mislead one to a wrong conclusion about better sensitivity of the more

recent experiments. There is generally some possible incorrectness in the direct comparison of the exclusion curves for the WIMP–proton(neutron) spin-dependent cross section obtained with and without the nonzero WIMP–neutron(proton) spin-dependent contribution. Furthermore, the above-mentioned incorrectness concerns to a great extent the direct comparison of spin-dependent exclusion curves obtained with and without nonzero spin-independent contributions [46,47]. Taking into account both spin couplings a_p and a_n but ignoring the scalar coupling c_0, one can easily arrive at a misleading conclusion especially for not very light target nuclei when it is not obvious that (both) spin couplings dominate over the scalar one. To be consistent, one has to use a mixed spin–scalar coupling approach as for the first time proposed by the DAMA Collaboration [44,46,47].

It was argued in [44,46,47,51,52] that potentially misleading discrepancies between the results of different dark matter search experiments (for example, DAMA vs. CDMS and EDELWEISS), as well as between the data and the SUSY calculations can be avoided by using the mixed spin–scalar coupling approach, where the spin-independent and spin-dependent WIMP–nucleon couplings are a priori considered to be *both* nonzero.

The mixed spin–scalar coupling approach was applied to analyze the data from both HDMS experiments with natural Ge and with the neutron-odd group high-spin isotope ^{73}Ge. The approach allows both upper limits for spin-dependent $\sigma_{\rm SD}^{n(p)}$ and spin-independent $\sigma_{\rm SI}$ cross sections of WIMP–nucleon interaction to be simultaneously determined from the experimental data. In this way visible improvement in the form of exclusion curves is achieved relative to the traditional one-coupling dominance scheme [93]. The agreement of the obtained $\sigma_{\rm SD}^{n}$ and $\sigma_{\rm SI}$ with the parameter regions allowed from the observation of the annual modulation signature by the DAMA Collaboration is demonstrated. The above-mentioned correlations between $\sigma_{\rm SD}^{n}$ and $\sigma_{\rm SI}$ can be considered as a new requirement, which demands that for any fixed WIMP mass m_χ one should have $\sigma_{\rm SI}(\text{theor.}) \leqslant \sigma_{\rm SI}(\text{fitted})$ and $\sigma_{\rm SD}^{n}(\text{theor.}) \leqslant \sigma_{\rm SD}^{n}(\text{fitted})$, simultaneously, provided $\sigma_{\rm SD(SI)}^{n(p)}(\text{theor.})$ are calculated in any underlying SUSY-like theory. For the first time a similar result for NaI was mentioned by the DAMA Collaboration [45].

It is important to note, that without proper knowledge of the nuclear and nucleon structure it is not possible to extract reliable and useful information (at least in the form of these $\sigma_{\rm SD}^{n}$ and $\sigma_{\rm SI}$ cross sections) from direct dark matter search experiments. However, astrophysical uncertainties, in particular the DM distribution in vicinity of the Earth [53–59], make the problem of interpretation of the results of the DM search experiments far more complicated. At the moment to have a chance to compare sensitivities of different experiments people adopted one common truncated Maxwellian DM particle distribution, but nobody can prove its correctness. Only in the case of indeed direct DM detection one can

make some conclusions about the real DM particle distribution in the vicinity of the Earth.

Furthermore, almost by definition (from the very beginning), a modern experiment aiming at the best exclusion curve is doomed to nonobservation of the DM signal. This is due to the fact, that a typical expected DM-signal spectrum exponentially drops with recoil energy, and it is practically impossible to single it out from a background non-WIMP spectrum of a typical (semiconductor) detector, which is as usual exponential as well.

In fact, one needs some clear, or «positive» signature of WIMP particle interactions with target nuclei. Only exclusion curves are not enough. Ideally this signature should be a unique feature of such an interaction (see, for example, [158]).

There are some typical characteristics of WIMP particle interactions with a nuclear target which can potentially play the role of such positive WIMP signatures (see, for example, [159]). First of all, WIMPs produce nuclear recoils, while most radioactive backgrounds produce electron recoils. Nevertheless, for example, neutrons (and any other heavy neutral particle) also can produce nuclear recoils. There exist also some proposals which rely on WIMP detection via electron recoils (see, for example, [160–162]).

Due to the extremely rare event rate of the WIMP–nuclear interactions (the mean free path of a WIMP in matter is of the order of a light-year) one can expect two features. The first one is that the probability of two consecutive interactions in a single detector or two closely located detectors is completely negligible. Multiple interactions of photons, gamma rays or neutrons under the same conditions are much more common. Therefore only nonmultiple interaction events can pretend to be from WIMPs. The second one is a uniform distribution of the WIMP induced events throughout a detector. This feature can also be used *in future* to identify background events (from photons, neutrons, beta and alpha particles) in rather large-volume position-sensitive detectors.

The shape of the WIMP-induced recoil energy spectrum can be predicted rather accurately (for given WIMP mass, for fixed nuclear structure functions and astrophysical parameters). The observed energy spectrum, pretending to be from WIMPs, must be consistent with the expectation. However, this shape is exponential, right as it is the case for many background sources.

Obviously, the nuclear-recoil feature, the nonmultiple interaction, the uniform event distribution throughout a detector and the shape of the recoil energy spectrum could not be a clear «positive signature» of WIMP interactions. One believes that the following three features of WIMP–nuclear interaction can serve as a clear «positive signature».

The currently most promising, technically reachable and already used (by the DAMA Collaboration) «positive signature» is the annual modulation signature. The WIMP flux and its average kinetic energy vary annually due to the combined

motions of the Earth and Sun relative to the galactic center. The impact WIMP energy increases (decreases) when the Earth velocity is added to (subtracted from) the velocity of the Sun. The amplitude of the annual modulation depends on many factors — the details of the halo model, mass of the WIMP, the year-averaged rate (or total WIMP–nuclear cross sections), etc. In general the expected modulation amplitude is rather small (see, for example, [26,27] and [46,47]) and to observe it one needs huge (at best ton scale) detectors which can continuously operate over 5–7 years. Of course, to reliably use this signature one should prove the absence of annually-modulated backgrounds. One should, however, also be aware that seasonal modulation can also originate from other scenarios such as caustic rings of axions or neutralinos in the halo dark matter distribution [163, 164].

Another potentially promising positive WIMP signature is connected with the possibility of measuring the direction of the recoil nuclei induced by a WIMP. In these directional recoil experiments one plans to measure the correlation of the event rate with the Sun motion (see, for example, [87, 161, 165]). Unfortunately, the task is extremely complicated (see, for example, [81–85]).

The third well-known potentially useful positive WIMP signature is connected with the coherence of the WIMP–nucleus spin-independent interaction. Due to a rather low momentum transfer a WIMP coherently scatters on the whole target nucleus and the elastic cross section of this interaction should be proportional to A^2, where A is the atomic number of the target nucleus. Contrary to the A^2 behavior, the cross section of neutron scattering on nuclei (due to the strong nature of this interaction) is proportional to the geometrical cross section of the target nucleus ($A^{2/3}$-dependence). To reliably use this A^2 signature one has to satisfy at least two conditions. First, one should be sure that the spin-independent WIMP–nuclear interaction indeed dominates over the relevant spin-dependent interaction. This is far from being obvious (see, for example, [51,69,90,166,167]). Second, one should, at least, for two targets with different atomic number A rather accurately measure the recoil spectra (in the worst case integrated event rates) under the same background conditions. Currently this goal looks far from being realizable.

Developing further the idea of this third signature, one can also consider as a possible extra WIMP signature an observation of the similarity (or coherent behavior) of measured spectra at different (also nonzero spin) nuclear targets. This possibility relies on rather accurate spin structure functions for the experimentally interesting nuclei (see, for example, [70, 99]).

Also in the case of currently very promising event-by-event active background reduction techniques (like in the CDMS and EDELWEISS experiments) one inevitably needs clear positive WIMP signature(s). Without these signatures one hardly can convince anyone that the final spectrum is saturated only by WIMPs. Furthermore, with the help of these extra signatures one can define the WIMP mass from the spectrum [168, 169].

It is known (see, for example, the discussion in [39] and earlier partly in [124]) that a proof of the observation of a dark matter signal is an extremely complicated problem. As was pointed out above, on this way an interpretation of measurements in the form of exclusion curves helps almost nothing. Of course, an exclusion curve is at least something from nothing observed. It allows sensitivity comparison of different experiments and therefore allows one to decide which at the moment is the best «excluder». But, for example, supersymmetric theory is, in general, very flexible, it has a lot of parameters, and one hardly believes that an exclusion curve can ever impose any decisive constraint on it. The situation is much worse due to the already mentioned famous nuclear and astrophysical uncertainties involved in the exclusion curves evaluation [86, 140, 170–175]. This is why, from our point of view, it is not very decisive (or wise) to use very refined data and methods (nuclear, astrophysical, numerical, statistical [176], etc.) and spend big resources fighting only for the best exclusion curve. This fighting could only be accepted, perhaps, in the case when one tries to strongly improve the sensitivity of a small detector having future plans to use many copies of it in a huge detector array with a total ton-scale mass.

As has already been stressed in [79,150], in case of a positive DM signal, e.g., the detector HDMS has no means to discriminate the signal from background. With a target mass of 200 g only, the statistical accuracy within 2 years of measurements is too low in order to see the annual modulation, which is nowadays the only available positive signature of WIMP interaction with terrestrial matter. The same is completely true for any other potentially very accurate low-target-mass direct dark matter search experiment. To have a chance to see the annual modulation signature of WIMP–nuclear interaction and to detect dark matter particles, as seems to have been done by DAMA, one preferably needs either a GENIUS-like huge setup [177, 178] which was planned to operate up to 1000 kg of HPGe detectors of different enrichment of ^{76}Ge and ^{73}Ge (in a large volume of ultra-pure liquid nitrogen), or, perhaps, a setup with a bit smaller mass, which is able to perform permanent data taking over at least several years under extremely low background conditions (like, for example, the GENIUS-TF experiment [179, 180], or a future enlarged EDELWEISS setup). The performing of such an experiment seems, however, more difficult than originally expected [181–184].

CONCLUSION

In this review paper the following main questions have been discussed.

Why do we want to improve the exclusion curves? The answer usually is: to constrain a SUSY-like theory. Unfortunately this is an almost hopeless aim due to the huge flexibility of such theories and the inevitable necessity of extra information from other SUSY-sensitive observables (for example, from LHC, or

Tevatron). Almost all experimental groups presenting their exclusion curves try to compare them with some SUSY predictions. It is clear from this comparison (see, for example, Fig. 7) that there are some domains of the SUSY parameter space, which are excluded already now by these exclusion curves. What is remarkable, however, is that nobody yet has seriously considered — or used otherwise — these constraints for SUSY. In short, at the present and foreseeable level of experimental accuracy, simple fighting for the best exclusion curve is almost useless, either for real DM detection, or for substantial restrictions for SUSY.

How far can one improve an exclusion curve? It is almost a question of taste, when one should decide to stop speculations on the improvement of the exclusion curve. Almost always one can find something to improve the exclusion curve.

What would one like to see in the future beyond an exclusion curve? New generations of dark matter experiments right from their beginning *should aim at detection* of dark matter particles. This will require development of new setups, which will be able to register *positive signatures* of the dark matter particle interactions with nuclear targets. At least the DAMA [44–47] and LIBRA [60, 185] experiments are seen on the way. In order to be convincing, an eventual WIMP signal should combine more than one of these positive WIMP signatures [158, 159].

Why should one try to obtain a real recoil energy spectrum? The spectrum allows one to look for the annual modulation effect, the only nowadays available positive dark matter signature, which can prove existence of dark matter particle interactions with terrestrial nuclei. There are also attempts to determine the WIMP mass on the basis of measured recoil spectra [168, 169]. Very accurate off-line investigation of the measured spectrum allows one to single out different non-WIMP background sources and to perform controllable background subtractions.

It seems that, at the level of our present knowledge, the dark matter problem could not be solved independently from other related problems (proof of SUSY, astrophysical dark matter properties, etc.). Furthermore, due to the huge complexity (technical, physical, astrophysical, necessity for positive signatures, etc.) to solve the problem of dark matter one should not be afraid, but openly use a reliable model-dependent framework — for example, the framework of SUSY, where the same LSP neutralino should be seen coherently or lead to effects in all available experiments (direct and indirect DM searches, rare decays, high-energy searches at LHC, etc.). Only if such SUSY framework leads to a specific and decisive positive WIMP signature, this could mean a proof of SUSY and simultaneous solution of the dark matter problem. It is, on the other hand, absolutely clear that SUSY, although in contrast to others being preferrred, since requested by «higher» particle physics theories, such as Superstrings, is not the only candidate for the origin of dark matter, and also other scenarios have to be investigated in a comparably thorough way.

This work was supported by the RFBR (grant 06-02-04003) and DFG (grant 436 RUS 113/679/0-2(R)). The authors thank Dr. I. V. Krivosheina for the long-term and very fruitful collaboration, and Dr. E. A. Yakushev (JINR) for useful discussions.

REFERENCES

1. *Zwicky F.* // Helv. Phys. Acta. 1933. V. 6. P. 110–127.
2. *Freeman K.* // Science. 2003. V. 302, No. 5652. P. 1902–1903.
3. *Mosher D.* http://www.space.com/scienceastronomy/070510_dark_dwarfs.html
4. *Bertone G., Hooper D., Silk J.* // Phys. Rep. 2005. V. 405. P. 279–390; hep-ph/0404175.
5. *Kamionkowski M.* astro-ph/0706.2986.
6. *Salucci P.* astro-ph/0707.4370.
7. *Yao W. M. et al.* // J. Phys. G. 2006. V. 33. P. 1–1232.
8. *Bergstrom L.* // Rep. Prog. Phys. 2000. V. 63. P. 793; hep-ph/0002126.
9. *Kolb E. W.* astro-ph/0709.3102.
10. *Fukugita M., Peebles P. J. E.* // Astrophys. J. 2004. V. 616. P. 643–668; astro-ph/0406095.
11. *Bernardis P. et al.* // Nature. 2000. V. 404. P. 955–959; astro-ph/0004404.
12. *Balbi A. et al.* // Astrophys. J. 2000. V. 545. P. L1–L4; astro-ph/0005124.
13. *Linder E. V.* astro-ph/0801.2968.
14. *Lazkoz R.* // AIP Conf. Proc. 2007. V. 960. P. 3–32; astro-ph/0710.2872.
15. *Samtleben D., Staggs S., Winstein B.* // Ann. Rev. Nucl. Part. Sci. 2007. V. 57. P. 245–283; astro-ph/0803.0834.
16. *Klapdor H. V., Grotz K.* // Nuovo Cim. 1986. V. C9. P. 459–468.
17. *Klapdor H. V., Grotz K.* // Astrophys. J. 1986. V. L39. P. 304.
18. *Spergel D. N. et al.* // Astrophys. J. Suppl. 2003. V. 148. P. 175; astro-ph/0302209.
19. *Bennett C. L. et al.* // Ibid. P. 1; astro-ph/0302207.
20. *Komatsu E. et al.* astro-ph/0803.0547.
21. *Tegmark M. et al.* // Phys. Rev. D. 2006. V. 74. P. 123507; astro-ph/0608632.
22. *Percival W. J. et al.* // Astrophys. J. 2007. V. 657. P. 645–663; astro-ph/0608636.
23. *Tegmark M. et al.* // Phys. Rev. D. 2006. V. 73. P. 023505; astro-ph/0511774.
24. *Massey R. et al.* // Nature. 2007. V. 445. P. 286; astro-ph/0701594.
25. *Kamionkowski M., Kinkhabwala A.* // Phys. Rev. D. 1998. V. 57. P. 3256–3263; hep-ph/9710337.

26. *Freese K., Frieman J. A., Gould A.* // Phys. Rev. D. 1988. V. 37. P. 3388.
27. *Lewin J. D., Smith P. F.* // Astropart. Phys. 1996. V. 6. P. 87–112.
28. *Goodman M. W., Witten E.* // Phys. Rev. D. 1985. V. 31. P. 3059.
29. *Jungman G., Kamionkowski M., Griest K.* // Phys. Rep. 1996. V. 267. P. 195–373; hep-ph/9506380.
30. *Ellis J. R. et al.* // Phys. Rev. D. 2003. V. 67. P. 123502; hep-ph/0302032.
31. *Vergados J. D.* // J. Phys. G. 1996. V. 22. P. 253–272; hep-ph/9504320.
32. *Chattopadhyay U., Corsetti A., Nath P.* // Phys. Rev. D. 2003. V. 68. P. 035005; hep-ph/0303201.
33. *Bednyakov V. A., Klapdor-Kleingrothaus H. V., Kovalenko S.* // Phys. Rev. D. 1994. V. 50. P. 7128–7143; hep-ph/9401262.
34. *Bednyakov V. A., Klapdor-Kleingrothaus H. V., Kovalenko S. G.* // Phys. Rev. D. 1997. V. 55. P. 503–514; hep-ph/9608241.
35. *Bednyakov V. A., Klapdor-Kleingrothaus H. V.* // Phys. Rev. D. 2001. V. 63. P. 095005; hep-ph/0011233.
36. *Bednyakov V. A.* // Phys. At. Nucl. 2003. V. 66. P. 490–493; hep-ph/0201046.
37. *Bednyakov V. A., Klapdor-Kleingrothaus H. V.* // Phys. Rev. D. 1999. V. 59. P. 023514; hep-ph/9802344.
38. *Bednyakov V. A. et al.* // Z. Phys. A. 1997. V. 357. P. 339–347; hep-ph/9606261.
39. *Gondolo P.* hep-ph/0501134.
40. *Bertone G.* astro-ph/0710.5603.
41. *Hooper D., Baltz E. A.* hep-ph/0802.0702.
42. *Akerib D. S. et al.* astro-ph/0605719.
43. *Akimov D. Y.* // Instr. Exp. Tech. 2001. V. 44. P. 575–617.
44. *Bernabei R. et al.* // Phys. Lett. B. 2000. V. 480. P. 23–31.
45. *Bernabei R. et al.* // Phys. Lett. B. 2001. V. 509. P. 197–203.
46. *Bernabei R. et al.* // Riv. Nuovo Cim. 2003. V. 26. P. 1–73; astro-ph/0307403.
47. *Bernabei R. et al.* astro-ph/0311046.
48. *Alner G. J. et al.* // Phys. Lett. B. 2005. V. 616. P. 17–24; hep-ex/0504031.
49. *Cebrian S. et al.* // Nucl. Phys. Proc. Suppl. 2003. V. 114. P. 111–115; hep-ex/0211050.
50. *Yoshida S. et al.* // Nucl. Phys. Proc. Suppl. 2000. V. 87. P. 58–60.
51. *Bednyakov V. A., Klapdor-Kleingrothaus H. V.* // Phys. Rev. 2004. V. 70. P. 096006; hep-ph/0404102.
52. *Bednyakov V. A., Klapdor-Kleingrothaus H. V.* // Proc. of the 5th Intern. Heidelberg Conf. on Dark Matter in Astro and Particle Physics «DARK 2004», College Station, Texas, Oct. 3–9, 2004 / Eds. H.V. Klapdor-Kleingrothaus, R. Arnowitt. Berlin; Heidelberg, 2005. P. 583; hep-ph/0504031.

53. *Copi C. J., Krauss L. M.* // Phys. Rev. D. 2003. V. 67. P. 103507; astro-ph/0208010.

54. *Kurylov A., Kamionkowski M.* // Phys. Rev. D. 2004. V. 69. P. 063503; hep-ph/0307185.

55. *Tucker-Smith D., Weiner N.* // Phys. Rev. D. 2005. V. 72. P. 063509; hep-ph/0402065.

56. *Gelmini G., Gondolo P.* hep-ph/0405278.

57. *Savage C., Gondolo P., Freese K.* // Phys. Rev. D. 2004. V. 70. P. 123513; astro-ph/0408346.

58. *Gondolo P., Gelmini G.* // Phys. Rev. D. 2005. V. 71. P. 123520; hep-ph/0504010.

59. *Gelmini G. B.* // J. Phys. Conf. Ser. 2006. V. 39. P. 166–169; hep-ph/0512266.

60. *Bernabei R. et al.* // Eur. Phys. J. A. 2006. V. 27. P. 57–62.

61. *Sanglard V.* astro-ph/0612207.

62. *Akerib D. S. et al.* // Nucl. Instr. Meth. A. 2006. V. 559. P. 411–413.

63. *Brink P. L. et al.* astro-ph/0503583.

64. *Akimov D. Y. et al.* // Astropart. Phys. 2007. V. 27. P. 46–60; astro-ph/0605500.

65. *Lee. H. S. et al.* // Phys. Rev. Lett. 2007. V. 99. P. 091301; astro-ph/0704.0423.

66. *Engel J.* // Phys. Lett. B. 1991. V. 264. P. 114–119.

67. *Bottino A. et al.* hep-ph/0307303.

68. *Bednyakov V. A., Klapdor-Kleingrothaus H. V., Kovalenko S. G.* // Phys. Lett. B. 1994. V. 329. P. 5–9; hep-ph/9401271.

69. *Bednyakov V. A.* // Phys. At. Nucl. 2004. V. 67. P. 1931–1941; hep-ph/0310041.

70. *Bednyakov V. A., Simkovic F.* // Part. Nucl. 2005. V. 36. P. 131–152; hep-ph/0406218.

71. *Girard T. A. et al.* // Phys. Lett. B. 2005. V. 621. P. 233–238; hep-ex/0505053.

72. *Girard T. A. et al.* hep-ex/0504022.

73. *Giuliani F.* // Phys. Rev. Lett. 2004. V. 93. P. 161301; hep-ph/0404010.

74. *Giuliani F., Girard T. A.* // Phys. Rev. D. 2005. V. 71. P. 123503; hep-ph/0502232.

75. *Benoit A. et al.* // Phys. Lett. B. 2005. V. 616. P. 25–30; astro-ph/0412061.

76. *Tanimori T. et al.* // Phys. Lett. B. 2004. V. 578. P. 241–246; astro-ph/0310638.

77. *Moulin E., Mayet F., Santos D.* // Phys. Lett. B. 2005. V. 614. P. 143–154; astro-ph/0503436.

78. *Mayet F. et al.* // Phys. Lett. B. 2002. V. 538. P. 257; astro-ph/0201097.

79. *Klapdor-Kleingrothaus H. V., Krivosheina I. V., Tomei C.* // Phys. Lett. B. 2005. V. 609. P. 226–231.

80. *Ovchinnikov B. M., Parusov V. V.* The Preparing of an Experiment for Search the Spin-Dependent Interactions of WIMP. INR Preprint 1097/2003. 2003.

81. *Alner G. J. et al.* // Nucl. Instr. Meth. A. 2004. V. 535. P. 644–655.

82. *Snowden-Ifft D. P., Martoff C. J., Burwell J. M.* // Phys. Rev. D. 2000. V. 61. P. 101301; astro-ph/9904064.

83. *Gaitskell R. J. et al.* // Nucl. Instr. Meth. A. 1996. V. 370. P. 162–164.

84. *Sekiya H. et al.* astro-ph/0405598.

85. *Morgan B., Green A. M., Spooner N. J. C.* // Phys. Rev. D. 2005. V. 71. P. 103507; astro-ph/0408047.

86. *Vergados J. D.* // Part. Nucl., Lett. 2001. V. 106. P. 74–108; hep-ph/0010151.

87. *Vergados J. D.* // Phys. At. Nucl. 2003. V. 66. P. 481–489; hep-ph/0201014.

88. *Divari P. C. et al.* // Phys. Rev. C. 2000. V. 61. P. 054612.

89. *Bednyakov V. A., Klapdor-Kleingrothaus H. V., Kovalenko S. G.* // Phys. Rev. D. 1997. V. 55. P. 503–514; hep-ph/9608241.

90. *Bednyakov V. A.* // Part. Nucl. 2007. V. 38. P. 326–363.

91. *Klapdor-Kleingrothaus H. V. et al.* // Astropart. Phys. 2003. V. 18. P. 525–530; hep-ph/0206151.

92. *Klapdor-Kleingrothaus H. V. et al.* hep-ph/0103077.

93. *Bednyakov V. A., Klapdor-Kleingrothaus H. V., Krivosheina I.* // Phys. At. Nucl. 2008. V. 71. P. 111–116.

94. *Smith P. F., Lewin J. D.* // Phys. Rep. 1990. V. 187. P. 203.

95. *Bednyakov V. A., Klapdor-Kleingrothaus H. V.* // Phys. At. Nucl. 1999. V. 62. P. 966–974.

96. *Bednyakov V. A., Kovalenko S. G., Klapdor-Kleingrothaus H. V.* // Phys. At. Nucl. 1996. V. 59. P. 1718–1727.

97. *Engel J., Pittel S., Vogel P.* // Intern. J. Mod. Phys. E. 1992. V. 1. P. 1–37.

98. *Ressell M. T. et al.* // Phys. Rev. D. 1993. V. 48. P. 5519–5535.

99. *Bednyakov V. A., Simkovic F.* // Part. Nucl. 2006. V. 37. P. S106–S128; hep-ph/0608097.

100. *Engel J. et al.* // Phys. Rev. C. 1995. V. 52. P. 2216–2221; hep-ph/9504322.

101. *Ressell M. T., Dean D. J.* // Phys. Rev. C. 1997. V. 56. P. 535–546; hep-ph/9702290.

102. *Griest K.* // Phys. Rev. D. 1988. V. 38. P. 2357.

103. *Ellis J. R., Flores R. A.* // Nucl. Phys. B. 1988. V. 307. P. 883.

104. *Ellis J. R., Flores R. A.* // Phys. Lett. B. 1991. V. 263. P. 259–266.

105. *Engel J., Vogel P.* // Phys. Rev. D. 1989. V. 40. P. 3132–3135.

106. *Iachello F., Krauss L. M., Maino G.* // Phys. Lett. B. 1991. V. 254. P. 220–224.

107. *Nikolaev M. A., Klapdor-Kleingrothaus H. V.* // Z. Phys. A. 1993. V. 345. P. 373–376.

108. *Dimitrov V., Engel J., Pittel S.* // Phys. Rev. D. 1995. V. 51. P. 291–295; hep-ph/9408246.

109. *Ellis J. R., Flores R. A.* // Nucl. Phys. B. 1993. V. 400. P. 25–36.

110. *Bernabei R. et al.* astro-ph/0305542.

111. *Drukier A. K., Freese K., Spergel D. N.* // Phys. Rev. D. 1986. V. 33. P. 3495–3508.

112. *Pacheco A. F., Strottman D.* // Phys. Rev. D. 1989. V. 40. P. 2131–2133.

113. *Engel J. et al.* // Phys. Lett. B. 1992. V. 275. P. 119–123.

114. *Kosmas T. S., Vergados J. D.* // Phys. Rev. D. 1997. V. 55. P. 1752–1764; hep-ph/9701205.

115. *Tovey D. R. et al.* // Phys. Lett. B. 2000. V. 488. P. 17–26; hep-ph/0005041.

116. *Mandic V. et al.* hep-ph/0008022.

117. *Bergstrom L., Gondolo P.* // Astropart. Phys. 1996. V. 5. P. 263–278; hep-ph/9510252.

118. *Gondolo P.* hep-ph/0005171.

119. *Bottino A. et al.* // Phys. Rev. D. 2001. V. 63. P. 125003; hep-ph/0010203.

120. *Ellis J. R. et al.* hep-ph/0308075.

121. *Bednyakov V. A., Klapdor-Kleingrothaus H. V., Gronewold V.* // Phys. Rev. D. 2002. V. 66. P. 115005; hep-ph/0208178.

122. *Bednyakov V. A., Klapdor-Kleingrothaus H. V., Zaiti E.* // Ibid. P. 015010; hep-ph/0203108.

123. *Bednyakov V. A.* hep-ph/0208172.

124. *Bednyakov V. A., Klapdor-Kleingrothaus H. V.* // Phys. Rev. D. 2000. V. 62. P. 043524; hep-ph/9908427.

125. *Hagiwara K. et al.* // Phys. Rev. D. 2002. V. 66. P. 010001.

126. *Alam M. S. et al.* // Phys. Rev. Lett. 1995. V. 74. P. 2885–2889.

127. *Abe K. et al.* hep-ex/0107065.

128. *Bertolini S. et al.* // Nucl. Phys. B. 1991. V. 353. P. 591–649.

129. *Barbieri R., Giudice G. F.* // Phys. Lett. B. 1993. V. 309. P. 86–90; hep-ph/9303270.

130. *Buras A. J. et al.* // Nucl. Phys. B. 1994. V. 424. P. 374–398; hep-ph/9311345.

131. *Ali A., Greub C.* // Z. Phys. C. 1993. V. 60. P. 433–442.

132. *Gondolo P. et al.* astro-ph/0012234.

133. *Bednyakov V. A., Klapdor-Kleingrothaus H. V., Tu H.* // Phys. Rev. D. 2001. V. 64. P. 075004; hep-ph/0101223.

134. *Drees M., Nojiri M.* // Phys. Rev. D. 1993. V. 48. P. 3483–3501; hep-ph/9307208.

135. *Bottino A. et al.* // Phys. Lett. B. 1997. V. 402. P. 113–121; hep-ph/9612451.

136. *Ahmed B. et al.* // Astropart. Phys. 2003. V. 19. P. 691–702; hep-ex/0301039.

137. *Akerib D. S. et al.* // Phys. Rev. Lett. 2004. V. 93. P. 211301; astro-ph/0405033.

138. *Sanglard V.* astro-ph/0406537.

139. *Chardin G.* astro-ph/0411503.

140. *Copi C. J., Krauss L. M.* // Phys. Rev. D. 2001. V. 63. P. 043507; astro-ph/0009467.

141. *Drees M.* hep-ph/0410113.

142. *Miuchi K. et al.* // Astropart. Phys. 2003. V. 19. P. 135–144; astro-ph/0204411.

143. *Giuliani F., Girard T. A.* // Phys. Lett. B. 2004. V. 588. P. 151–154; astro-ph/0311589.

144. *Takeda A. et al.* // Phys. Lett. B. 2003. V. 572. P. 145–151; astro-ph/0306365.

145. *Bernabei R. et al.* // Nucl. Phys. Proc. Suppl. 2002. V. 110. P. 88–90.

146. *Bernabei R. et al.* // Phys. Lett. 1998. V. B436. P. 379–388.

147. *Bernabei R. et al.* // Nucl. Instr. Meth. A. 2002. V. 482. P. 728–743.

148. *Ellis J. R., Ferstl A., Olive K. A.* // Phys. Lett. B. 2000. V. 481. P. 304–314; hep-ph/0001005.

149. *Klapdor-Kleingrothaus H. V. et al.* hep-ph/0103082.

150. *Tomei C.* PhD Thesis. Univ. of L'Aquila, Italy, 2004.

151. *Baudis L. et al.* // Phys. Rev. D. 1999. V. 59. P. 022001; hep-ex/9811045.

152. *Garcia E. et al.* // Phys. Rev. D. 1995. V. 51. P. 1458–1464.

153. *Baudis L. et al.* // Nucl. Instr. Meth. A. 1999. V. 426. P. 425–435; hep-ex/9811040.

154. *Akerib D. S. et al.* // Phys. Rev. D. 2006. V. 73. P. 011102; astro-ph/0509269.

155. *Alner G. J. et al.* // Astropart. Phys. 2005. V. 23. P. 444–462.

156. *Benoit A. et al.* // Phys. Lett. B. 2006. V. 637. P. 156–160; astro-ph/0512120.

157. *Bednyakov V. A., Simkovic F.* // Phys. Rev. D. 2005. V. 72. P. 035015; hep-ph/0506195.

158. *Spooner N. J.* astro-ph/0705.3345.

159. *Gascon J.* astro-ph/0504241.

160. *Vergados J. D., Ejiri H.* // Phys. Lett. B. 2005. V. 606. P. 313–322.

161. *Vergados J. D.* astro-ph/0411126.

162. *Vergados J. D., Quentin P., Strottman D.* // Intern. J. Mod. Phys. E. 2005. V. 14. P. 751; hep-ph/0310365.

163. *Sikivie P.* // Proc. of «Beyond the Desert 99»: Accelerator, Nonaccelerator and Space Approaches, Ringberg Castle, Tegernsee, Germany, June 6–12, 1999 / Eds. H. V. Klapdor-Kleingrothaus, I. V. Krivosheina. IOP. Bristol and Philadelphia, 1999. P. 547.

164. *Sikivie P.* // Proc. «Beyond the Desert 2003»: Accelerator, Nonaccelerator and Space Approaches, Ringberg Castle, Tegernsee, Germany, June 9–14, 2003 / Ed. H. V. Klapdor-Kleingrothaus. Heidelberg; N. Y., 2004. P. 601; astro-ph/0309627.

165. *Vergados J. D.* // Phys. Rev. D. 2003. V. 67. P. 103003; hep-ph/0303231.

166. *Vergados J. D.* hep-ph/0512305.

167. *Vergados J. D.* // J. Phys. G. 2004. V. 30. P. 1127–1144; hep-ph/0406134.

168. *Green A. M.* // JCAP. 2007. V. 0708. P. 022; hep-ph/0703217.

169. *Shan C.-L., Drees M.* hep-ph/0710.4296.

170. *Kinkhabwala A., Kamionkowski M.* // Phys. Rev. Lett. 1999. V. 82. P. 4172–4175; astro-ph/9808320.

171. *Donato F., Fornengo N., Scopel S.* // Astropart. Phys. 1998. V. 9. P. 247–260; hep-ph/9803295.

172. *Evans N. W., Carollo C. M., Zeeuw P. T.* // Mon. Not. Roy. Astron. Soc. 2000. V. 318. P. 1131; astro-ph/0008156.

173. *Green A. M.* // Phys. Rev. D. 2001. V. 63. P. 043005; astro-ph/0008318.

174. *Green A. M.* // Phys. Rev. D. 2002. V. 65. P. 023520; astro-ph/0106555.

175. *Ullio P., Kamionkowski M.* // JHEP. 2001. V. 03. P. 049; hep-ph/0006183.

176. *Feldman G. J., Cousins R. D.* // Phys. Rev. D. 1998. V. 57. P. 3873–3889; physics/9711021.

177. *Klapdor-Kleingrothaus H. V., Hirsch M.* // Z. Phys. A. 1997. V. 359. P. 361–372.

178. *Hellmig J., Klapdor-Kleingrothaus H. V.* // Ibid. P. 351–359; nucl-ex/9801004.

179. *Tomei C. et al.* // Nucl. Instr. Meth. A. 2003. V. 508. P. 343–352; hep-ph/0306257.

180. *Klapdor-Kleingrothaus H. V. et al.* // Nucl. Instr. Meth. A. 2002. V. 481. P. 149–159; hep-ex/0012022.

181. *Klapdor-Kleingrothaus H. V. et al.* // Nucl. Instr. Meth. A. 2003. V. 511. P. 341–346; hep-ph/0309170.

182. *Klapdor-Kleingrothaus H. V. et al.* // Nucl. Instr. Meth. A. 2004. V. 530. P. 410–418.

183. *Klapdor-Kleingrothaus H. V., Krivosheina I. V.* // Nucl. Instr. Meth. A. 2006. V. 566. P. 472–476.

184. *Krivosheina I. V., Klapdor-Kleingrothaus H. V.* // Phys. Scripta. 2006. V. T127. P. 52–53.

185. *Bernabei R. et al.* // Phys. At. Nucl. 2006. V. 69. P. 2056–2067.